International Journal of Refractory Metals and Hard Materials,
Volume 69, December 2017, Pages 215-226
DOI: 10.1016/j.ijrmhm.2017.08.017

Manuscript Details

Manuscript number	IJRMHM_2017_451
Title	Elevated temperature repetitive micro-scratch testing of AlCrN, TiAlN and AlTiN PVD coatings
Article type	Research Paper

Abstract

In developing advanced wear-resistant coatings for tribologically extreme highly loaded applications such as high speed metal cutting a critical requirement is to investigate their behaviour at elevated temperature since the cutting process generates frictional heat which can raise the temperature in the cutting zone to 700-900 °C or more. High temperature micro-tribological tests provide severe tests for coatings that can simulate high contact pressure sliding/abrasive contacts at elevated temperature. In this study ramped load micro-scratch tests and repetitive micro-scratch tests were performed at 25 and 500 °C on commercial monolayer coatings (AlCrN, TiAlN and AlTiN) deposited on cemented carbide cutting tool inserts. AlCrN exhibited the highest critical load for film failure in front of the moving scratch probe at both temperatures but it was prone to an unloading failure behind the moving probe. Scanning electron microscopy showed significant chipping outside the scratch track which was more extensive for AlCrN at both room and elevated temperature. Chipping was more localised on TiAlN although this coating showed the lowest critical loads at both test temperatures. EDX analysis of scratch tracks after coating failure showed tribo-oxidation of the cemented carbide substrate. AlTiN showed improved scratch resistance at higher temperature. The von Mises, tensile and shear stresses acting on the coating and substrate sides of the interface were evaluated analytically to determine the main stresses acting on the interface. At 1 N there are high stresses near the coating-substrate interface. Repetitive scratch tests at this load can be considered as a sub-critical load micro-scale wear test which is more sensitive to adhesion differences than the ramped load scratch test. The analytical modelling showed that a dramatic improvement in the performance of AlTiN in the 1 N test at 500 °C could be explained by the stress distribution in contact resulting in a change in yield location due to the high temperature mechanical properties. The increase in critical load with temperature on AlTiN and AlCrN is primarily a result of the changing stress distribution in the highly loaded sliding contact rather than an improvement in adhesion strength.

Keywords	scratch test; elevated temperature; nanomechanics; AlCrN; AlTiN

Corresponding Author	Ben Beake
Corresponding Author's Institution	Micro Materials Ltd
Order of Authors	Ben Beake, Jose Luis Endrino, Christine Kimpton, german fox-rabinovich, Stephen Veldhuis

Submission Files Included in this PDF

File Name [File Type]

Covering letter.docx [Cover Letter]

Research Highlights.docx [Highlights]

REV HT Micro-wear paper v1e.docx [Manuscript File]

Fig 1.tif [Figure]

Fig 2a.tif [Figure]

Fig 2b.tif [Figure]

Fig 3a AlCrN 500C scr.tif [Figure]

Fig 3b AlCrN 500C wear+BSE inset.tif [Figure]

Fig 3c TiAlN 500C scr.tif [Figure]

Fig 3d TiAlN 500C wear.tif [Figure]

Fig 4a.tif [Figure]

Fig 4b.tif [Figure]

Fig 4c.tif [Figure]

Fig 4d.tif [Figure]

Fig 5a.tif [Figure]

Fig 5b.tif [Figure]

Fig 5c.tif [Figure]

Fig 6.tif [Figure]

Fig 7a 4340 end milling.tif [Figure]

Fig 7b 1040 AlCrN end milling.tif [Figure]

Fig 7c 1040 face milling.tif [Figure]

To view all the submission files, including those not included in the PDF, click on the manuscript title on your EVISE Homepage, then click 'Download zip file'.

Research Data Related to this Submission

There are no linked research data sets for this submission. The following reason is given:
Data will be made available on request

Research Highlights

- Wear behaviour of hard nitride coatings in repetitive micro-scratch tests was highly temperature-sensitive
- The wear mechanism in repetitive scratch tests depends on whether plastic flow starts in coating or substrate
- Differences in scratch critical load with temperature are due to changing stress distributions not adhesion

Elevated temperature repetitive micro-scratch testing of AlCrN, TiAlN and AlTiN PVD coatings

B.D. Beake[1]*, J.L. Endrino[2], C. Kimpton[2], G.S. Fox-Rabinovich[3] and S.C. Veldhuis[3]

1 Micro Materials Ltd, Willow House, Yale Business Village, Ellice Way, Wrexham, LL13 7YL, UK

2 SENTi, School of Aerospace, Transport and Manufacturing, Cranfield University, Bedford, MK43 0AL, UK

3 Department of Mechanical Engineering, McMaster University, 1280 Main Street West, Hamilton, Ontario L8S 4L7, Canada

* Corresponding author. Tel: +44 1978 261615, Fax: +44 1978 356966. Email: ben@micromaterials.co.uk

Keywords: scratch test; elevated temperature; nanomechanics; AlCrN; AlTiN

Abstract

In developing advanced wear-resistant coatings for tribologically extreme highly loaded applications such as high speed metal cutting a critical requirement is to investigate their behaviour at elevated temperature since the cutting process generates frictional heat which can raise the temperature in the cutting zone to 700-900 °C or more. High temperature micro-tribological tests provide severe tests for coatings that can simulate high contact pressure sliding/abrasive contacts at elevated temperature. In this study ramped load micro-scratch tests and repetitive micro-scratch tests were performed at 25 and 500 °C on commercial monolayer coatings (AlCrN, TiAlN and AlTiN) deposited on cemented carbide cutting tool inserts. AlCrN exhibited the highest critical load for film failure in front of the moving scratch probe at both temperatures but it was prone to an unloading failure behind the moving probe. Scanning electron microscopy showed significant chipping outside the scratch track which was more extensive for AlCrN at both room and elevated temperature. Chipping was more localised on TiAlN although this coating showed the lowest critical loads at both test temperatures. EDX analysis of scratch tracks after coating failure showed tribo-oxidation of the cemented carbide substrate. AlTiN showed improved scratch resistance at higher temperature. The von Mises, tensile and shear stresses acting on the coating and substrate sides of the interface were evaluated analytically to determine the main stresses acting on the interface. At 1 N there are high stresses near the coating-substrate interface. Repetitive scratch tests at this load can be considered as a sub-critical load micro-scale wear test which is more sensitive to adhesion differences than the ramped load scratch test. The analytical modelling showed that a dramatic improvement in the performance of AlTiN in the 1 N test at 500 °C could be explained by the stress distribution in contact resulting in a change in yield location due to the high temperature mechanical properties. The increase in critical load

with temperature on AlTiN and AlCrN is primarily a result of the changing stress distribution in the highly loaded sliding contact rather than an improvement in adhesion strength.

Introduction

Metal cutting generates frictional heat which can raise the temperature in the cutting zone to in excess of 700 °C [1-2]. In developing advanced coatings for metal cutting applications a key requirement is therefore to investigate their behaviour at elevated temperature. Sophisticated high temperature test techniques are now being employed to characterise the properties of advanced wear-resistant coatings [3-4]. We have previously shown how high temperature nanomechanical characterisation can be a valuable tool in understanding coating properties and how they will perform in different types of cutting tests with different requirements [4-5]. Tribological tests at high temperature also show that the test temperature plays a key role in determining wear rate and deformation mechanism [6-11]. Coated components in machining applications operate in the region of their elastic limit, or above it as stresses in cutting can be 2 GPa or more [2,12] so it also desirable to mimic these high stresses in the laboratory tests. This can be done by elevated temperature nano- and micro-scale tribological tests which extend the characterisation capability and provide severe tests of coating durability that can simulate highly loaded sliding/abrasive contacts at elevated temperature.

The scratch test is a convenient method for producing damage to simulate abrasive wear [13-14] and a popular choice for coating adhesion assessment [15]. However, it is well known that critical loads in the scratch test do not directly correspond to more adherent films since the critical load is dependent on many factors in addition to the interfacial strength [16-17]. Another limitation is that when scratching thin wear resistant hard coatings with a 200 μm radius diamond probe the maximum von Mises stresses move deep into the substrate before failure occurs [18-19].

One way to increase the sensitivity of the test to interfacial adhesion is to reduce the probe size and use a nano- or micro-scratch test instrument with greater sensitivity at lower load. By "dimensioning" the test in this way the influence of substrate deformation is reduced [18]. Hertzian modelling can provide an estimate of the mean contact pressure and location of the peak von Mises stress in the scratch test [20]. Depending on the choice of indenter radius and load, the maximum stress can be positioned at the interface, or at interfaces between different layers in a multi-layer coating system, to investigate any potential deficiencies in adhesion. Further control over the contact pressure and the location of maximum stress is achieved by performing repetitive (sub-critical load) constant load nano- and micro- scratch tests. With a suitable choice of applied load it is possible to study either coating-dominated wear properties or interfacial behaviour, as has been done previously at the nano- and micro-scales for hard carbon and nitride coatings [20-21]. The micro-scale scratch test can be considered as a model single asperity contact where the major abrasive wear mechanisms can be well reproduced [13-14]. Studying single asperity contact at the nano- [22-23] or micro- [14] scale has distinct advantages compared to standard tribological tests with much larger contact sizes. In these tests the real contact occurs only at the peaks of the asperities and the actual contact pressures responsible for the observed behaviour are not known.

In this study the micro-scale scratch and wear behaviour of three industrial coatings, TiAlN, AlCrN and AlTiN, popularly used in metal cutting has been investigated at room and elevated temperatures. The main aims of the study were to (i) apply Hertzian and analytical modelling approaches to improve our understanding of the micro-scratch and micro-wear tests at room temperature (ii) interpret differences in coating behaviour in terms of their mechanical properties (iii) apply the same approach to the coating behaviour in tests at elevated temperature (iv) investigate possible correlations with metal cutting tests. Analytical modelling of the von Mises stress distribution in the sliding contact was performed to

investigate how differences in coating mechanical properties at high temperature affect the initial interface weakening (i.e. by initial substrate or coating yielding or both) and determine the observed deformation failure mechanism.

2. Experimental

2.1 Materials

Three commercially available coatings of the same thickness, fabricated in a standard Balzers RCS cathodic arc coating machine, were investigated in this study: TiAlN (X-treme), AlTiN (X-ceed) and AlCrN (Alcrona). The Al to Ti/Cr ratio is 0.5 in TiAlN, 0.67 in AlTiN and 0.7 in AlCrN. The monolayer columnar coatings were deposited on mirror polished Sandvik H1P cemented carbide inserts (SPG422) to a thickness of (3.0 ± 0.2) μm. TiAlN and AlCrN have a cubic structure while the AlTiN has a dual phase cubic and wurtzite structure which results in lower hardness and elastic modulus. The coatings have compressive residual stress in the range -3 to -4 GPa. The chemical composition of the cemented carbide substrate material was: WC = 85.5; TiC = 7.5; TaC = 1.0; Co = 6.0 wt.%. Their mechanical properties were measured by nanoindentation testing with a NanoTest system (Micro Materials Ltd., Wrexham, UK) at 25 and 500 °C using a high temperature stage and separately actively heated diamond Berkovich indenter, as summarised in Table 1(a) [24, 25]. Grain sizes were larger on the TiAlN than the AlCrN and AlTiN [26-28].

2.2 Micro-scratch testing

Ramped load micro-scratch testing to a peak load of 10 N was performed with a NanoTest system (Micro Materials Ltd, Wrexham, UK) using a 3-scan procedure using a spheroconical diamond indenter with an end radius of 25 μm. The procedure involved 3 sequential scans,

topography-scratch-topography, at 5 μm/s. These were (i) pre-scan: scanning at low load over a 1000 μm track (no wear occurs at this load with a 25 μm probe) (ii) progressive load scratch: the load is low over the first 250 μm scan then ramping at a constant rate of 75 mN/s to reach 10 N just before the end of the scan (iii) post-scan, with the same low load as the pre-scan. The scans were always in the same direction and the probe was removed from the surface at the end of each scan. At least 3 scratch tests were done on each sample, with adjacent tracks separated by 200 μm. R_a surface roughness was 0.03-0.04 μm on AlTiN and 0.05-0.06 μm on AlCrN and TiAlN. Based on the results of the ramped load scratch tests, various constant loads (0.5-4 N) were chosen for multi-pass constant load repetitive micro-scratch tests (micro-wear) tests that were performed over 1000 μm in a similar manner. In these 12-scan tests the pre-scan was followed by 10 wear cycles under load, loading at 150 mN/s after 250 μm scan distance to reach the peak load rapidly (at 300-350 μm scan distance depending on load) remaining at this level until the end of the scan, before a final post-scan to determine the residual depth. The scans were always in the same direction and the probe was removed from the surface at the end of each scan. The evolution of wear was followed by changes to the depth measured under load (the on-load wear depth) and the R_a surface roughness.

For the high temperature micro-scratch tests the instrument was stabilised at the test temperature of 500 °C prior to testing. The final thermal drift minimisation process before starting the scan involved holding the diamond probe in contact with the coating surface at minimal force for 30 s, passively heating the probe. The 500 °C repetitive scratch tests were performed at 1 and 2 N on AlTiN, and at 1 N on TiAlN and AlCrN. In the figures that follow, the depth data in the ramped load scratch and repetitive scratch tests are shown after removal of the slope, topographic and the instrument compliance contribution to the measured

deformation, to leave true depth data [16,29]. The mean pressure during the tests was estimated by the application of a Hertzian treatment previously applied to nano- and micro-scratch tests with spherical probes [15-16]. The method enables the yield stresses and the pressure required for the failure of the film to be estimated from contact mechanics, assuming the geometry of indentation, provided spherical indenters are used and assuming elastic recovery. The contact depth (h_c) in a spherical indentation contact is given by

$$h_c = (h_t + h_r)/2 \qquad \text{[Eqn. 1]}$$

where h_c is the contact depth, h_t is the on-load scratch depth and h_r is the residual depth from the final scan. The contact radius (a) is determined from Equation 2, where R is the indenter radius. The contact pressure, P_m, at any point along the scratch track is given by equation 3, where L is the applied load.

$$a = \sqrt{(2Rh_c - h_c^2)} \qquad \text{[Eqn. 2]}$$

$$P_m = L/\pi a^2 \qquad \text{[Eqn. 3]}$$

When the scratch load increases beyond the elastic limit and significant plasticity and ploughing friction occurs the above treatment is no longer exact but nevertheless can provide a useful indication of both the contact pressure and the depth at which the maximum von Mises stress is likely to be found ($0.48a$) and hence in deciding a suitable load for the sub-critical load repetitive scratch tests.

Secondary electron and back scattered imaging of coating surfaces after micro-scratch testing was performed with an Oxford Instruments SEM fitted with an EDX detector.

2.3 Analytical modelling

The von Mises, tensile and shear stresses acting on the coating and substrate sides of the interface were evaluated using the SAC (simple adhesion calculator) in the SIO Toolbox (SIO, Rugen, Germany) which uses Film Doctor (SIO, Rugen, Germany) analytical methodology to determine the main stresses acting on the interface for a single-layer coating system. The input parameters to the model are the mechanical properties of the coating and substrate at the test temperature i.e. hardness (H), elastic modulus (E), the ratio of hardness to yield stress (Y), H/Y (taken as 1.5 for the coatings and 2.5 for the cemented carbide substrate), their Poisson ratios, together with the diamond indenter material properties and the applied load, friction coefficient and probe radius in the micro-scratch test. For the analysis the friction coefficient was set to 0.2, which is typical for hard nitride coatings sliding against 25 μm diamond probes. For the coatings the values shown in Table 1 were used and for the carbide those from references [30, 31]. Additionally, the Surface Stress Analyzer (SSA, from SIO) was used to provide a more detailed assessment of the stress distributions in the 1 N wear tests.

3. Results

3.1 Ramped load micro-scratch tests at 25 °C

As the load increased L_{c1} (= onset of cracking or unloading failure) and L_{c2} (= total failure in front of the probe) failures were observed. The critical load data from progressive load micro-scratch tests at 25 and 500 °C have previously been reported in [24,32] and are shown in Table 1(b). Hertzian analysis suggests that the maximum von Mises stress at the L_{c1} failure is located below the free surface, and moves further away from the coating-substrate interface by L_{c2} (Table 1(b)). An example of an unloading failure (i.e. a failure originating just behind the contact zone, resulting in extensive coating removal) on AlCrN is shown in figure 1. In the tests at 25 °C the unloading failure was seen predominantly on AlCrN, occasionally on AlTiN and was absent on TiAlN. There was significant chipping outside the scratch track which was more extensive for AlCrN.

3.2 Ramped load micro-scratch tests at 500 °C

The variation in scratch depth under load and residual scratch depth in the ramped tests at 500 °C are shown in figure 2 (a-b). The on-load depth was similar for all three coatings. Permanent deformation starts at lower load on AlTiN and, as the load increased was slightly greater on AlTiN and TiAlN than AlCrN. It can be seen from Table 1 that L_{c2} increases slightly with temperature for AlCrN and AlTiN but decreases for TiAlN. At the L_{c1} failure at 500 °C the maximum von Mises stress estimated by Hertzian mechanics is at a depth of around 4.5 μm for AlCrN, 3.6 μm for TiAlN and 6.3 μm for AlTiN. At the L_{c2} failure the maximum stress is at a depth of around 6.1 μm for AlCrN, 5.4 μm for TiAlN and 7.4 μm for the AlTiN. In tests at 500 °C the unloading failure was more common than at room temperature but occurred at higher load. It was present in every test on AlCrN, in 3 of 6 tests on TiAlN and only 1 of 6 repeats on AlTiN. At the start of the unloading failure the residual

depth is larger than the film thickness for AlCrN and AlTiN. Some plastic deformation of the cemented carbide substrate therefore occurred prior to coating failure. As at room temperature SEM imaging showed significant chipping outside the scratch track. This was more extensive for AlCrN (figure 3(a) than TiAlN (fig. 3(b)).

3.3 Constant load repetitive micro-scratch tests at 25 °C

The repetitive scratch depth data are summarised in Table 2. The depth during the initial pass under load at 1 N was almost the same for all three coatings. Illustrative constant load repetitive micro-scratch tests at 25 °C are shown in figure 4(a-d). The on-load depth includes the elastic deformation, so is greater than the residual wear depth which excludes it. Since the elastic contribution is expected to be approximately constant during the tests the on-load depth can provide a convenient assessment of the evolution of the wear with each subsequent scratch. For clarity only some of the wear cycles are shown. The deformation behaviour and the relative performance of the coatings were both highly load-dependent. After a few cycles at 1 N AlCrN worn regions along the scratch track were observed. Total coating failure occurred over 2/3 of the wear track by the 4th wear scan and was complete by the sixth scan (figure 4(a)). In the tests at 1 N AlTiN showed a mixture of low-wear areas and almost total coating removal in one test and minimal failure in the other (figure 4(b)), with lower scratch (elastic) recovery in the final post-scratch scan depth for the failed regions than the minimally worn regions. At 1 N (see figure 4(c)) and 2 N TiAlN exhibited a gradual fracture wear process without as abrupt an increase in depth. At 2 N the stress field calculations show the maximum von Mises stress moved to ~4 μm below the surface. The maximum contact pressure was estimated at 7.3-8.3 GPa at 1 N. At 2 N there was total coating failure over much of the wear track during the second or third scans on AlCrN and AlTiN. Figure 4(d) contrasts the behaviour on these coatings to TiAlN. After the coating was removed from the

scratch track the cemented carbide substrate was progressively worn away with each subsequent scratch pass. At ≥3 N the AlCrN coating was removed from the entire constant load region on the second wear cycle. The surface roughness measured under load was low, R_a = 0.06 μm at 3 N and R_a = 0.08 μm at 4 N. It remained unchanged between the first and second scans despite the increase in depth of nearly 4 μm for the second scan. The deformation under load on TiAlN was also very high but the residual depth was relatively low due to the inability of the probe to access the bottom of the scratch track.

3.4 Constant load repetitive micro-scratch tests at 500 °C

With each scratch TiAlN showed a gradual increase in on-load scratch depth with SEM imaging revealing some chipping outside the scratch track (figure 3(d)). AlCrN was initially wear resistant but after several cycles it failed over the majority of the wear track. It exhibited significant chipping outside the wear track (figure 3(c)). There were isolated regions outside the track where the coating was completely removed to reveal bare WC-Co as confirmed by EDX analysis. AlTiN did not fail during the 10 repeat scratches at 500 °C at 1 N. Increasing the wear load to 2 N produced similar behaviour to observed at room temperature, although a larger number of cycles were required to cause coating failure. EDX revealed the presence of oxygen (~18-20 wt.%) and Co enrichment (to ~13-14 wt.%) in the scratch tracks for the ramped load and 1 N repetitive scratch tests on AlCrN and TiAlN when the coating was removed. Oxygen was absent from the unworn regions of the coating surface and from chipped regions of the coating outside the scratch track. Compacted regions were observed over part of the wear tracks.

4. Discussion

4.1 Tribo-oxidation in the scratch tracks

The scratch and wear tests with the 25 μm diamond probe were highly loaded contacts with contact pressures in excess of 4 GPa. At these high pressures tribo-oxidation occurred in both room and elevated temperature tests as shown by the presence of oxygen in the scratch track after coating removal. 500 °C is below the normal oxidation onset temperature for these coatings. The coating surface and chipped regions of coating and bare substrate outside of the tracks themselves are oxide-free. Oxidation was reported by Staia and co-workers in the wear tracks from tribological tests of multi-layered and nanostructured TiAlN coatings at 500-700 °C [33]. The coatings were not worn through and the oxidation suggests a mixed tribolayer of Al_2O_3 and TiO_x. Outside of the wear tracks there was no detectable oxidation at these temperatures [33]. Oxidation of the Cobalt binder phase has been noted when bulk cemented carbide is subjected to repetitive micro-scratches at high contact pressure at room temperature [14]. Gee et al reported [14] fracture and fragmentation of WC-Co grains under repetitive sliding contact forming a nanostructured tribo-layer over surface as was observed in this study. This layer was found to be Co-rich by FIB-SIMS in agreement with the EDX results in this work. Tribo-oxidation has also been investigated in AFM experiments. Carpick and co-workers recently studied tribofilm formation when sliding an AFM tip in ZDDP-containing medium against Fe-containing or Si surfaces [22]. They reported that the rate of tribochemical reaction displayed an exponential dependence on contact pressure.

4.2 Ramped load scratch testing at 25 °C

It has been shown previously that a strong correlation exists between the mechanical properties of coatings (primarily hardness and H/E) and the scratch test critical load (L_{c2}) [16,17,20,34]. The nanoindentation data in Table 1 shows that at room temperature TiAlN was hardest at around 30 GPa, and AlTiN softest (20 GPa), with a significantly lower elastic modulus than the other two coatings [24,25]. Hard coatings with higher H/E are beneficial in providing load support but as the load increases stress relief by plastic flow is more critical. Failure in the scratch test is a brittle fracture dominated process at room temperature. Coatings with very high H/E can behave poorly due to their limited ductility, with reduced critical load. For hard coatings deposited on silicon there is more extensive delamination at failure [16,17,20,29], or chipping for harder DLC coatings on hardened steel [35]. Consistent with this general trend the smallest critical load was found for the hardest coating, TiAlN. The softer coatings AlCrN and AlTiN are able to more effectively relieve stress by plastic flow and hence higher resistance to cracking (see L_{c1} values in Table 1). Nevertheless, as the load increases unloading failures were observed. Unloading failures were also reported recently on other AlTiN and AlCrN coatings [36] but were absent when AlCrN was deposited as a bi-layer with a TiAlN sub-layer and in this study on TiAlN. AlCrN appears to be susceptible to dramatic fracture under highly loaded sliding contact if deposited without an adhesion-promoting layer, as has been observed by other groups [37]. The behaviour in the scratch test is controlled by mechanical properties with a contribution from microstructural effects. Grain refinement is promoted in high Al-fraction coatings [26]. The grain size is much smaller in the nanocrystalline AlTiN [26,28] and AlCrN [27] (~10-20 nm) than in TiAlN (~200 nm) [26] and this appears beneficial in reducing cracking.

It has been proposed [18] that plastic flow occurs wherever the critical von Mises stress is exceeded in the scratch test. With increasing load this plastic zone grows until it reaches the interface between the coating and the substrate. This weakens the integrity of the system. If

additionally high tensile stresses at the surface coincide with this weakening then mode-I fractures could propagate to this interface resulting in global coating failure by shearing off large areas at the observed critical load. In the micro-scratch test with a 25 μm probe end radius the compressive plastic strain in these coatings will be very small (of the order of a few % [38]), and so can be discounted when estimating the distance of the maximum von Mises stress to the coating-substrate interface [35]. The Hertzian analysis shows that the maximum von Mises stress is located in the substrate at L_{c1} for all three coatings and moves deeper as the load increases. This is consistent with the observation that when total coating failure occurs (e.g. see figure 1) the corresponding residual depth exceeds the coating thickness. The unloading failure is due to a high maximum tensile stress at the rear of the probe, as reported previously in scratch tests of hard DLC [39], TiSiN [28], $TiFeN_x$ [24,25] and TiN [40] coatings with 3-200 μm end radius probes.

4.3 Repetitive micro-scratch tests at 25 °C

In the ramped load scratch tests significant substrate deformation was required prior to L_{c1} failure of the coating systems. The role of substrate deformation can be investigated further in micro-wear tests at lower load where the behaviour is more coating-dominated and less influenced by the deformation of the substrate. The test probe radius and applied load in the scratch test control whether the initial scratch resistance is more strongly dependent on coating or substrate mechanical properties. The almost identical on-load depth during the first scratch at 1 N for the three different coatings (Table 2) reflects the dominant role of the substrate elastic properties in the measured deformation when using a 25 μm probe. This behaviour is strongly tip radius dependent. A radius of 25 μm has also been reported to effectively minimise differences in scratch resistance in micro-scratch tests on hard carbon coatings on tool steel [35] that were clear when the same coatings were scratched by a

sharper probe. The Hertzian stress model was used to estimate the contact pressures and the depth of the maximum von Mises stress in the test. The calculations show that at 1 N the maximum von Mises stress was at a depth of ~3 μm below the surface. Since the coatings are of 3 μm thickness and compressive strain is small the maximum stress was located in the vicinity of the coating-substrate interface. The repetitive micro-scratch test at this load should be more sensitive to the presence of any areas of weaker adhesion. The results of the analytical modelling show that the maximum von Mises stress on the substrate side of the interface at 1 N exceeds the substrate yield stress although there is no coating plasticity at this load. The maximum von Mises stresses determined by the Hertzian and analytical modelling approaches agree to within 10-15 % at 1 N. Since the system is overloaded, it is perhaps not surprising that failure was observed within a few scratch cycles even though the test load was below the L_{c1} critical load in the ramped load test. The different deformation mechanisms are consistent with microstructural differences with the Al-rich nanocrystalline coatings initially more wear resistant than the coarser grained TiAlN (figure 4(d)).

Analytical modelling was performed to determine the main stresses acting at the coating-substrate interface at 1 N and L_{c1}, L_{c2}. The results (Table 4) show that the maximum von Mises stresses were around 9 GPa and the maximum shear stresses were 3.5-3.9 GPa. At 25 °C although differences in coating mechanical properties affect the critical load, the mechanism is initial interface weakening by substrate yielding rather than coating failure which results in an abrupt “step” in scratch depth vs. load at failure. The slight reduction in the magnitude of the von Mises and shear stresses at the interface with increasing load are explained by the peak von Mises stresses moving further into the substrate as the scratch load increased.

The variation in the surface roughness in the scratch track with each repeat scratch can provide additional evidence of differences in deformation mechanisms. When measured under load over the entire constant load region, the evolution in R_a with each scratch pass provides a suitable metric. When deformation by plastic deformation is dominant with minimal wear from coating fracture in front of the probe then it will remain low. Significant fracturing or partial delamination during the scan will increase it. When complete failure occurs behind the probe then on the following wear cycle it stays low, consistent with carbide fracture requiring a number of repetitive scratches as reported by Gee and co-workers [14]. Although the initial scratch depths are essentially the same on all three coatings, differences in the evolution of the scratch depth and the surface roughness with repetitive scratches suggest that the subsequent wear process at ≥1 N proceeds by a different mechanism on TiAlN to the other coatings. In the first wear cycle the R_a roughness is higher than that measured at contact load on the coarser grained TiAlN implying some stress relief by cracking even at this load. For AlCrN and AlTiN it is identical, implying initially elastoplastic deformation without fracture. There is a correlation between the L_{c1} (and L_{c2}) values and the coating performance in the repetitive scratch tests at 1 N and 2 N. AlTiN has the highest L_{c1} of the three coatings at (3.5 ± 0.8) N so micro-fracture events are less likely at 1 N than on the other coatings. Severe deformation was observed in wear tests above 2 N (Table 2). Under these conditions the coating fails quickly and it is possible to monitor the damage tolerance of the system. For TiAlN 3 N is significantly above L_{c1} and so there is significant cracking during the first scratch resulting in higher surface roughness in the scratch track (R_a = 0.27 μm). For AlCrN 3 N was sufficiently close to the L_{c1} failure (2.8 ± 0.2 N) that dramatic failure occurred behind the probe during the first pass so that the probe depth was much deeper on the second pass. The absence of any change in on-load roughness confirms that failure occurs behind the probe in cycle 1. Complete coating failure exposes the

carbide substrate resulting in significant wear with increasing number of wear cycles. This is consistent with previous reports of scratching WC-Co showing plastic slip as the major mechanism followed by cracking and fragmentation of the individual WC grains after multiple passes [14].

4.4 Influence of temperature: ramped and repetitive micro-scratch tests at 500 °C

The ramped and repetitive micro-scratch tests are highly loaded contacts. A variety of dissipative mechanisms may be needed to reduce wear under these conditions with the elevated temperature mechanical properties of the system being paramount. The high temperature nanoindentation results on these coatings are summarised in Table 1. The data were taken from two studies with slightly different test conditions. The initial study on AlCrN and TiAlN used a short (5 s) hold at peak load that may not have been long enough to eliminate time-dependent effects during unloading, so that the reported values of elastic modulus – which were determined directly from the unloading slope without any viscoelastic correction [40] - may over-estimate the actual modulus of the coating. In the subsequent measurements on AlTiN the test protocol was improved with the addition of a longer hold period of 60 s at peak load before unloading. In hot microhardness testing in vacuum, Staia and co-workers reported that the rate of the hardness reduction with temperature on AlTiN (and to a lesser extent AlCrN) coatings was greater than the carbide substrate [33]. The nanoindentation data in refs [24,25] are in agreement with this.

The scratch and wear tests were dominated by brittle fracture behaviour at 25 °C. All the coatings soften at 500 °C which has been attributed to relaxation of residual stresses and grain boundary sliding [42]. The reduction in the hardness of coating and substrate at elevated temperature is consistent with greater plasticity, and consequently in milder deformation behaviour in the scratch test. The reduction in hardness of the carbide substrate was not

measured in this study but has been reported elsewhere to decrease only slightly by 500 °C [30]. Pujante and co-workers reported that for AlCrN on tool steel, with and without prior surface hardening by nitriding, the critical load reduced with temperature due to substrate softening [43]. Allsopp and Hutchings reported that at 350 °C (a temperature where softening of the tool steel substrate is less pronounced) the critical load for AlTiN on tool steel was considerably higher than at room temperature [44].

The mechanisms of stress relief are predominantly by plastic flow on AlTiN and plastic flow and micro-fracture on TiAlN. The observed differences in both on-load (elastic and plastic) and residual (plastic) depths between the coatings are consistent with differences in their high temperature hardness (Table 1(a)). The unloading failure on AlCrN may be related to its higher hot hardness, so that less efficient stress relief is possible by plastic flow. It does not necessarily imply worse adhesion at higher temperature since a high load (and higher bending stresses) were required for the coating to fail at 500 °C than at 25 °C. The temperature dependence of the critical load in Table 4 is primarily a result of the different stress distribution rather than an improvement in adhesion strength at high temperature. The analytically determined maximum shear stress at the L_{c2} failure is higher at 25 °C than 500 °C which suggests the coating-substrate bonding strength is slightly reduced at high temperature. Although the shear stress is much lower at failure on the AlTiN coating the failure mechanism at elevated temperature is different (as discussed below), so it is not possible to directly compare its adhesion strength at high temperature to the other coatings. Unloading failures in micro-scratch tests occurred more often on AlTiN after vacuum annealing for 2 h at 900 °C [45]. The annealing increased the high temperature hardness of AlTiN but reduced the critical load, but at higher temperature the critical load was higher for as-deposited and annealed samples than at room temperature [45].

In the tests at 500 ºC there are high stresses in the vicinity of the coating-substrate interface, with maximum von Mises stress at 1 N estimated by Hertzian mechanics at a depth of 3 μm below the surface (i.e. very close to the interface, assuming the coatings deform elastically). For TiAlN, L_{c1} and L_{c2} are lower at 500 ºC than at 25 ºC, and its poorer wear performance in the repetitive scratches at 1 N at 500 ºC compared to 25 ºC is consistent with this. In contrast AlCrN and AlTiN show improved performance, with more cycles required before failure and lower residual depth. The lower residual depth is likely to be due to reduced fracturing of the WC-Co which also softens slightly at 500 ºC [30]. The improved behaviour of the AlTiN coating at 1 N may be related to its significantly higher L_{c1} at 500 ºC. The enhanced ductility for AlTiN is consistent with the maximum von Mises stress moving further into the substrate at L_{c1} than at 25 ºC.

Analytical modelling of the main stresses acting at the coating-substrate interface (using SIO Toolbox, SIO, Germany) was performed to investigate how the clear differences in coating high temperature mechanical properties (Table 1) influence the initial interface weakening (i.e. by initial substrate or coating yielding or both) and thus determine the deformation failure mechanism at elevated temperature. The results show that differences in the coating behaviour in the 1 N tests at 500 ºC between AlTiN and the other coatings can be explained by differences in stress distributions at the interface. For all three coatings at 25 °C, and for AlCrN at 500 °C, the maximum von Mises stress on the substrate side of the interface at 1 N exceeds the substrate yield stress although there is no coating plasticity at this load. For TiAlN at 500 °C the interface is weakened by a combination of plastic flow of coating and substrate. The reported elastic modulus of AlCrN at 500 ºC is considered to be an over-estimate of the true value due to the holding time at peak load (5 s) being too short. The stress analysis was therefore re-run with a lower value of 510 GPa. The values given in Table 4 were unchanged. In contrast, for AlTiN at 500 °C there is plastic flow in the coating but the

von Mises stress in the substrate is much less than its yield stress (although this itself is lower at temperature). High H^3/E^2 is often associated with high fracture toughness and resistance to crack initiation. Although it has relatively low elastic modulus, the high L_{c1} on AlTiN at 500 °C is not due to having high H^3/E^2 since the other two coatings studied have higher H^3/E^2. Instead it is a consequence of lower interfacial stresses, plastic flow in the coating and reduced substrate deformation. The Surface Stress Analyzer (from SIO) provided a more detailed assessment of the stress distributions in the 1 N wear tests at 500 °C. Figure 6 shows distributions of the von Mises stress for all three coatings. The simulated stress distributions support the conclusions from the Simple Adhesion Checker software, i.e. that a change in yield location and deformation mechanism can occur at high temperature due to the reduction in high temperature mechanical properties of the coatings.

4.5 Correlation with wear and cutting tests

Laboratory tests correlate well with actual application performance when there is accurate simulation of the contact conditions so that the severity and major deformation mechanisms can be replicated. The major deformation mechanisms in abrasive wear include plastic deformation, cutting, micro-fracture and delamination. These can be replicated in the scratch test but the critical load in the scratch test may not always be the best parameter for comparison. Bull has shown that the abrasive wear resistance for TiN coatings on 304 stainless steel deposited by different techniques did not show a good correlation with either the hardness or the critical load from a conventional scratch test [46]. More recently the nano-scale wear resistance of re-HIPed (HIP = hot Isostatically Pressed) and cast cobalt-based Stellite 6 alloys was investigated by Ahmed and co-workers with the nano-scratch test [47]. An excellent correlation between nano-scale wear resistance and results of the ASTM G65 abrasive wear test was found. The re-HIPed alloy showed lower material removal that was explained by differences in composition and properties of the metal matrix. The abrasive

wear resistance of AlTiN, AlCrN and TiAlN has been studied by Kalss and co-workers [48]. AlCrN showed significantly better abrasive wear resistance than AlTiN which was itself better than TiAlN. The high hardness of TiAlN confers load support but its relatively moderate plasticity results in low fracture resistance in highly loaded contact. With its larger grain size and columnar structure cracking results in high wear. The L_{c2} values from the room temperature micro-scratch test are consistent with the wear measurements in [48].

In cutting tests high stresses and temperatures exist in the contact zone. Temperatures can be in the range 700-1000 °C for continuous high speed cutting applications. In interrupted cutting of hard-to-cut materials such as Ti6Al4V they can be significantly lower, and depending on cutting speed may be well under 400 °C [49-51]. Although the micro-scale scratch tests at 500 °C cannot completely replicate some of the adaptive mechanisms operative at higher temperatures (e.g. age-hardening by spinodal decomposition, oxidation and tribo-film formation), nevertheless they can reveal differences in coating resistance to highly loaded sliding at high temperature that would not be predicted from tests at room temperature. In practice the results of the ramped and repetitive micro-scratch tests at 500 °C appear to show very good correlation with cutting tests. For example, figure 7 (a-c) shows illustrative cutting test data comparing tool life in face and end milling of steels taken from references [24-25]. In all three cases the high Al-fraction coatings, AlCrN and AlTiN outperform TiAlN in these applications. The high Al-fraction coatings also outperform TiAlN in a wider range of cutting conditions as illustrated by the tool-life data summarised in Table 5 [24,25, 48, 52-54]. The same trends have also been reported by other groups [e.g. 18, 37, 55, 56]. AlTiN has also shown moderate improvement over TiAlN in face milling of low carbon steel [56] and turning of medium carbon steel [18]. In face milling of 4140 steel Inspektor and Salvador reported a gradual improvement in tool life with increasing Al:Ti ratio [55]. Viana and co-workers noted that the relative performance of TiAlN and AlCrN

coated laser-textured cemented carbide tools in face milling of compacted graphite cast iron was dependent on cutting conditions [37]. More material removal was possible at low feed rate with TiAlN than with AlCrN coated tools. The relative performance switched round at higher feed rate. The authors interpreted these differences as being due to the temperature at the cutting edge. AlCrN coatings exhibit higher resistance to oxidation than $Ti_{1-x}Al_xN$ [24,48,49,54,57]. They suggest that at the lower rate the temperature would be sufficient for TiAlN oxidation but not AlCrN so that less effective tribo-film formation would be possible on the latter. However, the data in Table 1 suggest that differences in hardness reduction with temperature may also play a strong role. Chipping and delamination of AlCrN coatings can be mitigated by doping with functional elements such as Si or Y [55, 58] and addition of TiAlN bond layer [36] or insertion of TiN sublayers [57] to improve adhesion and tailor chromium out-diffusion respectively.

There are several reasons for the improved tool life in the higher Al-fraction coatings. They age-harden by spinodal decomposition more effectively than more Ti- or Cr- rich compositions [52, 59]. They form more protective alumina-based tribo-films than the less protective rutile and chromia tribofilms [54, 60]. They also have lower thermal conductivity at elevated temperature than TiAlN [48] which, with the tribo-film, has been shown to protect the tool from thermal softening [60], i.e. they can act as a thermal shield [31]. In applications requiring high hot hardness, such as continuous turning or end milling of hardened steel, AlTiN is outperformed by other Al-rich coatings with higher hot hardness. These include AlCrN, annealed AlTiN and more complex coatings such as TiAlCrN [61], TiAlCrSiYN [62] and TiAlCrSYN/TiAlCrN multilayers [60, 63]. Nevertheless, it possesses a higher L_{c1} at elevated temperature consistent with its reduced fracture in elevated temperature nano-impact tests [25]. AlTiN is preferable when the cutting conditions require relatively high coating plasticity, to minimise intensive adhesive-fatigue interaction with workpiece materials, as

occurs in machining strong aerospace materials Ti6Al4V, Ni-based superalloy (Waspalloy) or austensitic stainless steel [4]. The lower brittleness of the AlTiN coating helps provide more favourable, low wear conditions for effective tribo-film formation. This protects the cutting tool surface against chipping. The high temperature micro-scratch data (L_{c1} in the ramped tests and the repetitive tests at 1 or 2 N) on AlTiN, supported by the analytical modelling fully support this.

5. Conclusions

In this study ramped load micro-scratch tests and repetitive micro-scratch tests were performed at 25 and 500 °C on commercial monolayer coatings (AlCrN, TiAlN and AlTiN) deposited on cemented carbide cutting tool inserts.

In ramped load micro-scratch tests at 25 °C there was a lower critical load for TiAlN than AlCrN or AlTiN. The critical load decreased with temperature for TiAlN but increased for AlTiN and AlCrN. These results could be explained by differences in interfacial stress distributions caused by changing mechanical properties with coating composition, contact stress and temperature. The simulations showed that the temperature dependence of the micro-scratch test critical load is primarily a result of the changing stress distribution in the highly loaded sliding contact rather than an improvement in adhesion strength. In the repetitive scratch tests at 1 N at 25 and 500 °C the change in probe depth with number of scratch cycles could be used to monitor the wear process. AlTiN was more wear resistant than AlCrN and the wear process proceeded by a different mechanism on TiAlN. The analytical modelling showed that a dramatic improvement in the performance of AlTiN in the 1 N repetitive scratch test at 500 °C could be explained by the stress distribution in contact resulting in a change in yield location due to the high temperature mechanical properties.

The results of the high temperature ramped and repetitive micro-scratch tests are consistent with reported cutting test data. The high Al-fraction coatings AlCrN and AlTiN both can outperform TiAlN in a range of aggressive cutting conditions. Although it has relatively low elastic modulus, the high L_{c1} on AlTiN is not due to having high H^3/E^2 since the other two coatings studied have higher H^3/E^2. Instead it is a consequence of lower interfacial stresses, plastic flow in the coating and reduced substrate deformation, especially at 500 °C. This may explain its excellent performance in cutting materials, such as Ti6Al4V, where high temperature coating plasticity is more important than high temperature hardness.

6. References

1. N. Norrby, M. P. Johansson, R. M'Saoubi, M. Odén, Pressure and temperature effects on the decomposition of arc evaporated $Ti_{0.6}Al_{0.4}N$ coatings in continuous turning, Surf. Coat. Technol. 209 (2012) 203-207.
2. P. Wright, E.M. Trent, (2000) Metal Cutting, 4th Edition (Butterworth-Heinmann, Boston, USA).
3. M. Tkadletz, N. Schalk, R. Daniel, J. Keckes, C. Czettl, C. Mitterer, Advanced characterisation methods for wear resistant hard coatings: a review on recent progress, Surf. Coat. Technol. 285 (2016) 31-46.
4. B.D. Beake, G.S. Fox-Rabinovich, Progress in high temperature nanomechanical testing of coatings for optimising their performance in high speed machining, Surf. Coat. Technol. 255 (2014) 1021115.
5. B.D. Beake, G.S. Fox-Rabinovich, S.C. Veldhuis, S.R. Goodes, Coating optimisation for high-speed machining with advanced nanomechanical test methods, Surf. Coat. Technol., 203 (2009) 1919-1925.

6. K. Kutschej, P.H. Mayrhofer, M. Kathrein, P. Polcik, R. Tessadri, C. Mitterer, Structure, mechanical and tribological properties of sputtered coatings with $Ti_{1-x}Al_xN$ ($0.5 \leq x \leq 0.75$) Surf. Coat. Technol. 200 (2005) 2358-2365.
7. T. Polcar, R. Novak, P. Siroky, The tribological characteristics of TiCN coating at elevated temperatures, Wear 260 (2006) 40.
8. A. Pauschitz, M. Roy, F. Franek, Mechanisms of sliding wear of metals and alloys at elevated temperatures, Tribol. Int. 41 (2008) 584-602.
9. J. Veverkova, S.V. Hainsworth, Effect of temperature and counterface on the tribological properties of W-DLC on a steel substrate, Wear 264 (2008) 518-523.
10. O. Jantschner, C. Walter, C. Muratore, A.A. Voevodin, C. Mitterer, V-alloyed ZrO_2 coatings with temperature homogenization function for high-temperature sliding contacts, Surf. Coat. Technol. 228 (2013) 76-83.
11. A.A. Voevodin, C. Muratore, S.M. Aouadi, Hard coatings with high temperature adaptive lubrication and contact thermal management: review, Surface and Coating Technol. 257 (2014) 247-265.
12. K.-D. Bouzakis, N. Michailidis, G. Skordaris, E. Bouzakis, D. Biermann, R. M'Saoubi, Cutting with coated tools: coating technologies, characterization methods and performance optimisation, CRIP Ann. Manuf. Technol. 61 (2012) 703-723.
13. M.G. Gee, Low load multiple scratch tests of ceramics and hard metals, Wear 250 (2001) 264-281.
14. J.C.P. Zuñega, M.G. Gee, R.J.K. Wood and J. Walker, Scratch testing of WC/Co hardmetals, Tribol. Int. 54 (2012) 77-86.
15. ASTM C1624-05(2015), Standard Test Method for Adhesion Strength and Mechanical Failure Modes of Ceramic Coatings by Quantitative Single Point Scratch Testing.

16. B.D. Beake, V.M. Vishnyakov, and A.J. Harris, Relationship between mechanical properties of thin nitride-based films and their behaviour in nano-scratch tests, Tribol. Int. 44 (2011) 468-465.
17. B.D. Beake, V.M. Vishnyakov, A.J. Harris, Nano-scratch testing of (Ti,Fe)N_x thin films on silicon, Surf. Coat. Technol. 309 (2017) 671-679.
18. N. Schwarzer, Q.-H. Duong, N. Bierwisch, G. Favaro, M. Fuchs, P. Kempe, B. Widrig, J. Ramm, Optimisation of the scratch for specific coating designs, Surf. Coat. Technol. 206 (2011) 1327-1335.
19. C.T. Wang, A. Escudeiro, T. Polcar, A. Cavaleiro, R.J.K. Wood, Indentation and scratch testing of DLC-Zr coatings on ultrafine-grained titanium processed by high-pressure torsion, Wear 2013 (306) 304-310.
20. B. Shi, J.L. Sullivan, B.D. Beake, An investigation into which factors control the nanotribological behaviour of thin sputtered carbon films, J Phys D:Appl Phys 41 (2008) 045303.
21. B.D. Beake, B. Shi, J.L. Sullivan, Nanoscratch and nanowear testing of TiN coatings on M42 steel, Tribology 5 (2011) 141-147.
22. N.N. Gosvami, J.A. Bares, F. Mangolini, A.R. Konicek, D.G. Yablon, R.W. Carpick, Mechanisms of antiwear tribofilm growth revealed in situ by single asperity sliding contact, Science, 348 (2015) 102-106.
23. B. Bhushan, K.J. Kwak, Effect of temperature on nanowear of platinum-coated probes sliding against coated silicon wafers for probe-based recording technology, Acta Materialia 56 (2008) 380-386.
24. G.S. Fox-Rabinovich, B.D. Beake, S.C. Veldhuis, J.L. Endrino, R. Parkinson, L.S. Shuster, M.S. Migranov, Impact of mechanical properties measured at room and elevated

temperatures on wear resistance of cutting tools with TiAlN and AlCrN coatings, Surf. Coat. Technol. 200 (2006) 5738-5742.

25. B.D. Beake, J.F. Smith, A. Gray, G.S. Fox-Rabinovich, S.C. Veldhuis, J.L. Endrino, Investigating the correlation between nano-impact fracture resistance and hardness/modulus ratio from nanoindentation at 25-500ºC and the fracture resistance and lifetime of cutting tools with $Ti_{1-x}Al_xN$ (x=0.5 and 0.67) PVD coatings in milling operations, Surf. Coat. Technol. 201 (2007) 4585.
26. J.M. Anderson, J. Vetter, J. Müller, J. Sjölén, Structural effects of energy input growth of $Ti_{1-x}Al_xN$ ($0.55 \leq x \leq 0.66$) coatings by cathodic arc evaporation, Surf. Coat. Technol. 240 (2014) 211-220.
27. E. Le Bourhis, P. Goudeau, M.H. Staia, E. Carrasquero, E.S. Puchi-Cabrera, Mechanical properties of hard AlCrN-based coated substrates, Surf. Coat. Technol. 203 (2009) 2961-2968.
28. G.S. Fox-Rabinovich, J.L. Endrino, B.D. Beake, M.H. Aguirre, S.C. Veldhuis, DT Quinto, C.E. Bauer, A.I. Kovalev, A. Gray, Effect of annealing below 900°C on structure, properties and tool life of an AlTiN coating under various cutting conditions, Surf. Coat. Technol. 202 (2008) 2985.
29. B.D. Beake, V.M. Vishnyakov, R. Valizadeh, J.S. Colligon, Influence of mechanical properties on the nanoscratch behaviour of hard nanocomposite TiN/Si_3N_4 coatings on Si, J. Phys. D: Appl. Phys. 39 (2006) 1392-1397.
30. Yu.V. Milman, S. Luyckx, I.T. Northrop, Influence of temperature, grain size and cobalt content on the hardness of WC-Co alloys, Int. J. Refract. Met. Hard Mater. 17 (1999) 39-44.
31. I. Krajinović, W. Daves, M. Tkadletz, T. Teppernegg, T. Klünsner, N. Schalk, C. Mitterer, C. Tritremmel, W. Ecker, C. Czettl, Finite element study of the influence of

hard coatings on hard metal tool loading during milling, Surf. Coat. Technol. 304 (2016) 134-141.

32. A.J. Harris, B.D. Beake, D.E.J. Armstrong, Extreme nanomechanics: vacuum nanoindentation and nanotribology to 950 ºC, Tribology 9 (2015) 174-180.
33. M.H. Staia, M. D'Alessandria, D.T. Quinto, F. Roudet, M. Marsal Astort, High-temperature tribological characterisation of commercial TiAlN coatings, J. Phys.: Condens. Matter 18 (2006) S1727-S1736.
34. X.T. Xeng, S. Zhang, X.Z. Ding and D.G. Teer, Comparison of three types of carbon composite coatings with exceptional load-bearing capacity and high wear resistance, Thin Solid Films, 420-421 (2002) 36-370.
35. B.D. Beake, T.W. Liskiewicz, V.M. Vishnyakov, M.I. Davies, Development of DLC coating architectures for demanding functional surface applications through nano- and micro-mechanical testing, Surf. Coat. Technol. 284 (2015) 334-343.
36. B.D. Beake, L. Ning, C. Gey, S.C. Veldhuis, A. Komarov, A. Weaver, M. Khanna, G.S. Fox-Rabinovich, Wear performance of different PVD coatings during wet end milling of H13 tool steel, Surf. Coat. Technol. 279 (2015) 118-125.
37. R. Viana, M.S.F. de Lima, W.F. Sales, W.M. da Silva, A.R. Machado, Laser texturing of coated tools – performance during machining and in adhesion tests, Surf. Coat. Technol. 278 (2015) 485-501.
38. A.J. Haq, P.R. Munroe, M. Hoffman, P.J. Martin, A. Bendavid, Berkovich indentation of diamond like carbon coatings on silicon substrates, J. Mater. Res. 23 (2008) 1862-1869.
39. O. Borrero-López, H. Hoffman, A. Bendavid, P.J. Martin, Thin Solid Films 318 (2010) 4911-4917.
40. T. Chudoba, N. Schwarzer, F. Richter, Steps towards a mechanical modelling of layered systems, Surf. Coat. Technol. 154 (2002) 140-151.

41. G. Feng, A.H.W. Ngan, Effects of creep and thermal drift on modulus measurement using depth-sensing indentation, J. Mater. Res. 17 (2002) 660-668.
42. D.T. Quinto, G.J. Wolfe, P.C. Jinhal, High temperature microhardness of hard coatings produced by physical vapour deposition, Thin Solid Films 153, (1987) 19.
43. J. Pujante, M. Vilaseca, D. Casellas and M.D. Riera, High temperature scratch testing of hard PVD coatings deposited on surface treated tool steel, Surf. Coat. Technol. 257 (2014) 352-357.
44. D.N. Allsopp and I.M. Hutchings, Micro-scale abrasion and scratch response of PVD coatings at elevated temperatures, Wear 251 (2001) 1308-1314.
45. G.S. Fox-Rabinovich, J.L. Endrino, B.D. Beake, A.I. Kovalev, S.C Veldhuis, L. Ning, F. Fotaine, A. Gray, Impact of annealing on the microstructure, properties, and cutting performance of AlTiN coating, Surf. Coat. Technol. 201 (2006) 3524.
46. S.J. Bull, Can scratch testing be used as a model for the abrasive wear of hard coatings? Wear 233-235 (1999) 412-423.
47. R. Ahmed, A. Ashraf, M. Elameen, N.H. Faisal, A.M. El-Sherik, Y.O. Elakwak, M.F.A. Goosen, Single asperity nanoscratch behaviour of HIPed and cast Stellite 6 alloys, Wear 312 (2014) 70-82.
48. W. Kalss, A. Reiter, V. Derflinger, C. Gey, J.L. Endrino, Modern coatings in high performance cutting applications, Int. J. Refract. Met. Hard Mater. 24 (2006) 399-404.
49. N. Michailidis, Variations in the cutting performance of PVD-coated tools in milling Ti6Al4V, explained through temperature-dependent coating properties, Surf. Coat. Technol. 304 (2016) 325-329.
50. P. Zgorniak, A. Grdulska, Investigation of temperature distribution during milling process of Az91hp magnesium alloys, Mechanics and Mechanical Engineering, 16 (2012) 33-40.

51. U. Karaguzel, M. Bakkal, E. Budak, Modeling and measurement of cutting temperatures in milling, Procedia CIRP 46 (2016) 173-176.
52. J.L. Endrino, G.S. Fox-Rabinovich, C. Gey, Hard AlTiN, AlCrN PVD coatings for machining of austenitic stainless steel, Surf. Coat. Technol. 200 (2006) 6840-6845.
53. G.K. Dosbaeva, S.C. Veldhuis, K. Yamamoto, D.S. Wilkinson, B.D. Beake, N. Jenkins, A. Elfizy, G.S. Fox-Rabinovich, Oxide scales formation in nano-crystalline TiAlCrSiYN PVD coatings at elevated temperature, Int. J. Refract. Met. Hard Mater. 28 (2010) 133-141.
54. G.S. Fox-Rabinovich, K. Yamamoto, B.D. Beake, I.S. Gershman, A.I. Kovalev, S.C. Veldhuis, M.H. Aguirre, G. Dosbaeva, J.L. Endrino, Hierarchical adaptive nanostructured PVD coatings for extreme tribological applications: the quest for nonequilibrium states and emergent behaviour, Sci. Technol. Adv. Mater. 13 (2012) 043001 (26pp).
55. A. Inspektor and P.A. Salvador, Architecture of PVD coatings for metalcutting applications: a review, Surf. Coat. Technol. 257 (2014) 138-153.
56. A. Hörling, L. Hultman, M. Odén, J. Sjölén, L. Karlsson, Mechanical properties and machining performance of $Ti_{1-x}Al_xN$-coated cutting tools, Surf. Coat. Technol. 191 (2005) 384-392.
57. R. Escobar Galindo, J.L. Endrino, R. Martínez, J.M. Albella**,** Improving the oxidation resistance of AlCrN coatings by tailoring chromium out-diffusion**,** Spectrochim. Acta B, 65 (2010) 950-958
58. H. Scheerer and C. Berger, Wear Mechanisms of (Cr,Al,Y)N PVD Coatings at Elevated Temperatures, Plasma Processes and Polymers, S157-S161.

59. M. P. Johansson Jõesaar, N. Norrby, J. Ullbrand, R. M'Saoubi and M. Odén, Anisotropy effects on the microstructure and properties in decomposed evaporated Ti1-xAlxN coatings during metal cutting, Surf. Coat. Technol. 235 (2013) 181-185.
60. G.S. Fox-Rabinovich, J.L. Endrino, M.H. Agguire, B.D. Beake, S.C. Veldhuis et al, Mechanism of adaptability for the nano-structured TiAlCrSiYN-based hard physical vapor deposition coatings under extreme frictional conditions, J. Appl. Phys. 111 (2012) 064306.
61. G.S. Fox-Rabinovich, S.C. Veldhuis, G.K. Dosbaeva, K. Yamamoto, A.I. Kovalev, D.L. Wainstein, I.S. Gershman, L.S. Shuster, B.D. Beake, Nanocrystalline coating design for extreme applications based on the concept of complex adaptive behaviour, J. Appl. Phys. 103 (2008) 083510.
62. G.S. Fox-Rabinovich, S.C. Veldhuis, K. Yamamoto, MH. Aguirre, A. Kovalev, D.L. Wainstein, B.D. Beake, J.L. Endrino, D.L. Wainstein, A.Y. Rashkovskiy, Design and performance of AlTiN and TiAlCrN PVD coatings for machining of hard to cut materials, Surf. Coat. Technol. 204 (2009) 489-496.
63. B.D. Beake, G.S. Fox-Rabinovich, Y. Losset, K. Yamamoto et al, Why can TiAlCrSiYN-based adaptive coatings deliver exceptional performance under extreme frictional conditions? Faraday Discussions 156 (2012) 267-278.

Table 1. (a) Nanoindentation data at 25 and 500 ºC

Coating	Temperature (°C)	H (GPa)	E (GPa)	H/E	H^3/E^2 (GPa)
AlCrN	25	23.7	507	0.047	0.052
AlCrN	500	17.9	630	0.028	0.015
AlTiN	25	20.0	358	0.056	0.062
AlTiN	500	8.3	375	0.022	0.004
TiAlN	25	29.2	511	0.057	0.095
TiAlN	500	15.4	489	0.032	0.015
WC-Co	25	22	600	0.037	0.030
WC-Co	500	19	550	0.035	0.023

Mean values on the three coatings are taken from data with a Berkovich indenter previously reported in [24,32]. Values of E were determined using a Poisson's ratio of 0.25. The tests on AlCrN and TiAlN were at 25 mN with a 5 s hold at peak load before unloading. The tests on AlTiN were at 20 mN with a 60 s hold at peak load before unloading. Both sample and indenter were actively heated. WC-Co data are from references [30,31].

Table 1. (b) Critical loads in micro-scratch tests at 25 and 500 °C

Coating	Temperature (°C)	L_{c1} (N)	Depth of maximum Von Mises stress at L_{c1} (μm)	L_{c2} (N)	Depth of maximum Von Mises stress at L_{c2} (μm)	L_{c1}*[L_{c2}-L_{c1}] (N^2)
AlCrN	25	2.8 ± 0.2	4.5	5.7 ± 0.2	6.5	8.1
AlCrN	500	2.3 ± 0.4	4.5	6.0 ± 0.4	6.1	8.5
AlTiN	25	3.5 ± 0.8	5.7	4.5 ± 0.1	7.5	3.5
AlTiN	500	4.0 ± 0.6	6.3	5.8 ± 0.7	7.4	7.2
TiAlN	25	2.1 ± 0.4	4.5	4.2 ± 0.5	6.5	4.4
TiAlN	500	1.5 ± 0.2	3.6	3.7 ± 0.2	5.4	3.3

The critical load data were previously reported in [24] and [32]. L_{c1} = cohesive failure or unloading failure and L_{c2} = total failure in front of the probe. Data are from 3-6 tests. The depth of the maximum Von Mises stress is estimated from Hertzian mechanics.

Table 2. Constant load repetitive micro-scratch testing at 25 °C

Coating	Applied Load (N)	Depth under load in wear cycle 1 (μm)	Depth under load in wear cycle 10 (μm)	Increase in depth under load in 10 cycles (μm)	Residual depth (μm)
AlCrN	1.0	1.4 ± 0.1	4.9 ± 0.2	3.5 ± 0.3	3.9 ± 0.3
	2.0	2.1	7.6	5.5	5.6
	3.0	2.9	9.0	6.1	6.6
	4.0	3.6	11.3	7.7	7.9
AlTiN	1.0	1.4 ± 0	2.4 ± 1.0	0.9 ± 1.0	1.2 ± 0.9
	2.0	2.6 ± 0.2	7.9 ± 0.1	5.3 ± 0.2	5.8 ± 0.6
TiAlN	0.5	0.8	2.2	1.3	1.8
	1.0	1.5 ± 0.3	3.2 ± 0.4	1.7 ± 0.3	2.0 ± 0.7
	2.0	1.7	4.4	2.7	3.4
	3.0	3.9	7.2	3.3	2.7
	4.0	5.0	8.8	3.8	2.3

All depth data are mean values across the on-load region of the repetitive scratch track. The depth under load includes the contribution from elastic deformation. Where repeat tests were performed, the mean and the standard deviation are given.

Table 3. Constant load repetitive micro-scratch testing at 500 ºC

Coating	Applied Load (N)	Depth under load in wear cycle 1 (μm)	Depth under load in wear cycle 10 (μm)	Increase in depth under load in 10 cycles (μm)	Residual depth (μm)
AlCrN	1.0	1.2 ± 0.2	3.5 ± 0.2	2.3 ± 0.6	3.2 ± 0.5
AlTiN	1.0	1.2	1.5	0.2	0.5
	2.0	2.4 ± 0.1	5.3 ± 0.1	2.9 ± 0.1	4.9 ± 0.3
TiAlN	1.0	1.1 ± 0.0	3.1 ± 0.3	2.0 ± 0.3	2.6 ± 0.3

Data are mean values across the on-load region of the repetitive scratch track. The depth under load includes the contribution from elastic deformation. Where repeat tests were performed, the mean and the standard deviation are given.

Table 4 Estimated interfacial stresses at 1 N, L_{c1} and L_{c2}

(a) 25 °C

	Maximum von Mises stress (GPa)			Maximum shear stress (GPa)		
	at 1 N	at L_{c1}	at L_{c2}	at 1 N	at L_{c1}	at L_{c2}
AlCrN	8.9	8.9	8.8	3.5	3.8	3.9
AlTiN	9.1	8.8	8.8	3.6	3.9	3.9
TiAlN	8.9	8.9	8.9	3.5	3.8	3.9

(b) 500 °C

	Maximum von Mises stress (GPa)			Maximum shear stress (GPa)		
	at 1 N	at L_{c1}	at L_{c2}	at 1 N	at L_{c1}	at L_{c2}
AlCrN	7.8	7.7	7.6	3.1	3.2	3.4
AlTiN	4.4	4.7	4.6	1.9	2.1	2.2
TiAlN	7.9	7.8	7.7	3.1	3.2	3.4

Table 5 Comparative performance in cutting tool tests

Cutting Operation	Tool life			Reference
	TiAlN	AlTiN	AlCrN	
End milling 1040 steel	160 m		760 m	[24]
End milling 316 austenitic stainless steel		130 m #	90 m #	[52]
Hobbing case hardened 5115 steel		2300 parts	4100 parts	[48]
Interrupted turning 42CrMo4V steel	4000 strokes		6000 strokes	[48]
Face milling 1040 steel	2400 m	4500 m		[25]
End milling 4340 steel	86 m	104 m		[25]
End milling Ti6Al4V	6.1 m	10.3 m		[25]
Turning Inconel 718		320 m §	440 m §	[53]
Deep hole drilling of hardened structural steel	850 holes		1600 holes	[54]

Tool life defined as length of cut (m) until a tool flank wear of 300 μm was reached unless otherwise stated. # to flank wear of 100 μm. § to flank wear of 250 μm. Full cutting conditions are reported in the references.

Figure captions

1. Illustrative example of an unloading failure in a ramped load micro-scratch test on AlCrN at 25 °C.
2. (a) On-load scratch depth data at 500 ºC (including elastic deformation). (b) Residual depth data at 500 ºC (excluding elastic deformation).
3. SEM images of ramped and repetitive scratch tests at 500 ºC. The scratch direction is from right to left in all cases. (a) Ramped scratch at 500 ºC on AlCrN (b) ramped scratch at 500 ºC on TiAlN. Repetitive wear test at 1 N at 500 ºC on (c) AlCrN. The back-scattered image in the inset reveals carbide exposure outside the scratch track. (d) TiAlN. A lower magnification image of repeat tests is shown in the inset.
4. Repetitive micro-scratch tests at 1 N at 25 ºC; (a) TiAlN (b) AlTiN (c) AlCrN. (d) Comparison of wear depths during second scratch pass at 2 N 25 ºC.
5. Repetitive micro-scratch tests at 500 ºC (a) AlCrN at 1 N (b) AlTiN at 1 N (c) AlTiN at 2 N.
6. (a-c) Simulated von Mises stress distributions in the 1 N wear tests at 500 ºC. a = TiAlN; b = AlCrN; c = AlTiN. The scratch direction is from left to right.
7. Tool life flank wear data in cutting with coated cemented carbide inserts (i) end milling of 4340 steel with TiAlN and AlTiN (ii) end milling of 1040 steel with TiAlN and AlCrN (iii) face milling of 1040 steel with TiAlN and AlTiN. Full cutting conditions are given in references [24-25].

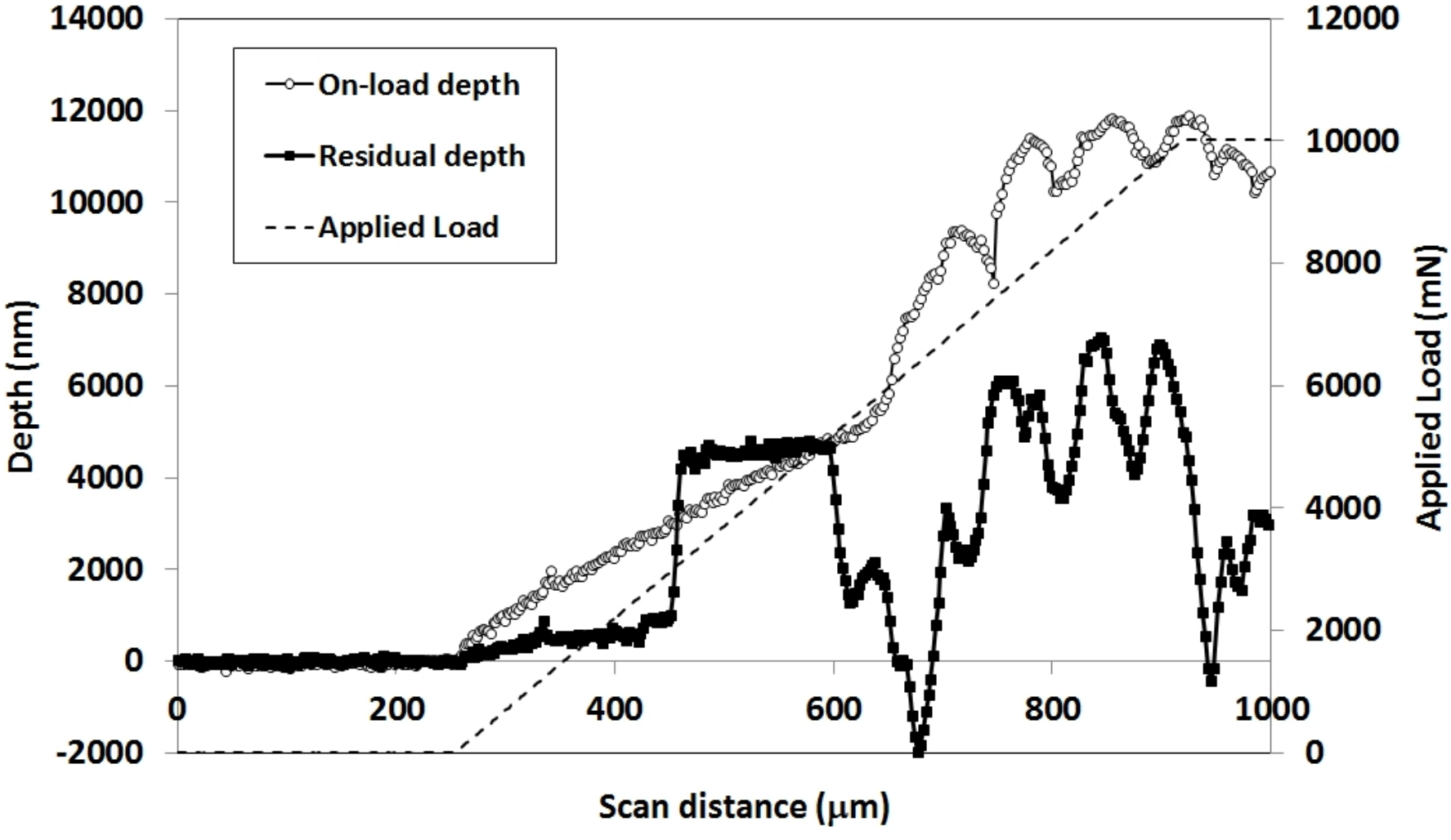
On-load depth
Residual depth
Applied Load
Depth (nm)
Applied Load (mN)
Scan distance (μm)
14000
12000
10000
8000
6000
4000
2000
0
-2000
12000
10000
8000
6000
4000
2000
0
0
200
400
600
800
1000

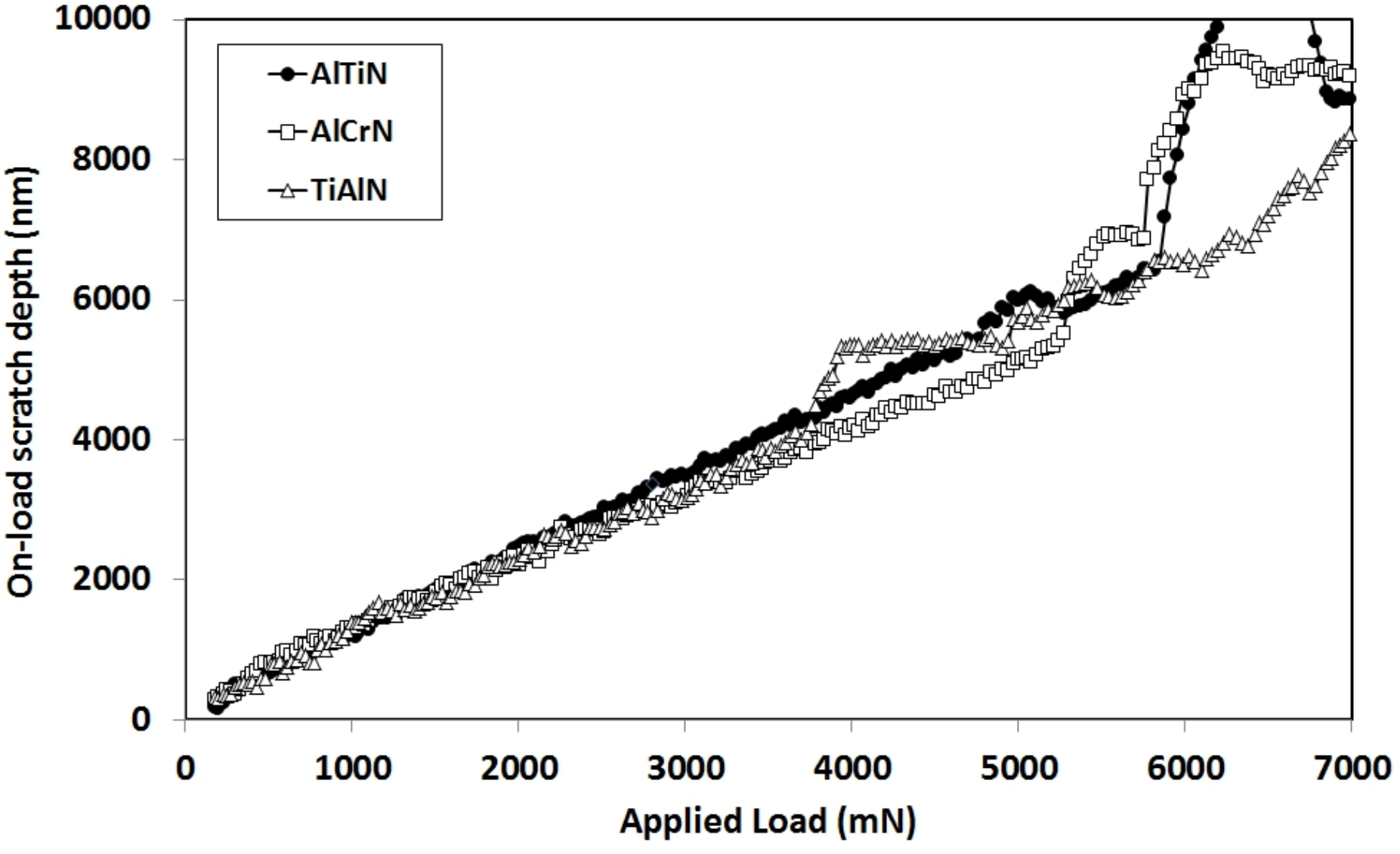
AlTiN
AlCrN
TiAlN
On-load scratch depth (nm)
10000
8000
6000
4000
2000
0
0
1000
2000
3000
4000
5000
6000
7000
Applied Load (mN)

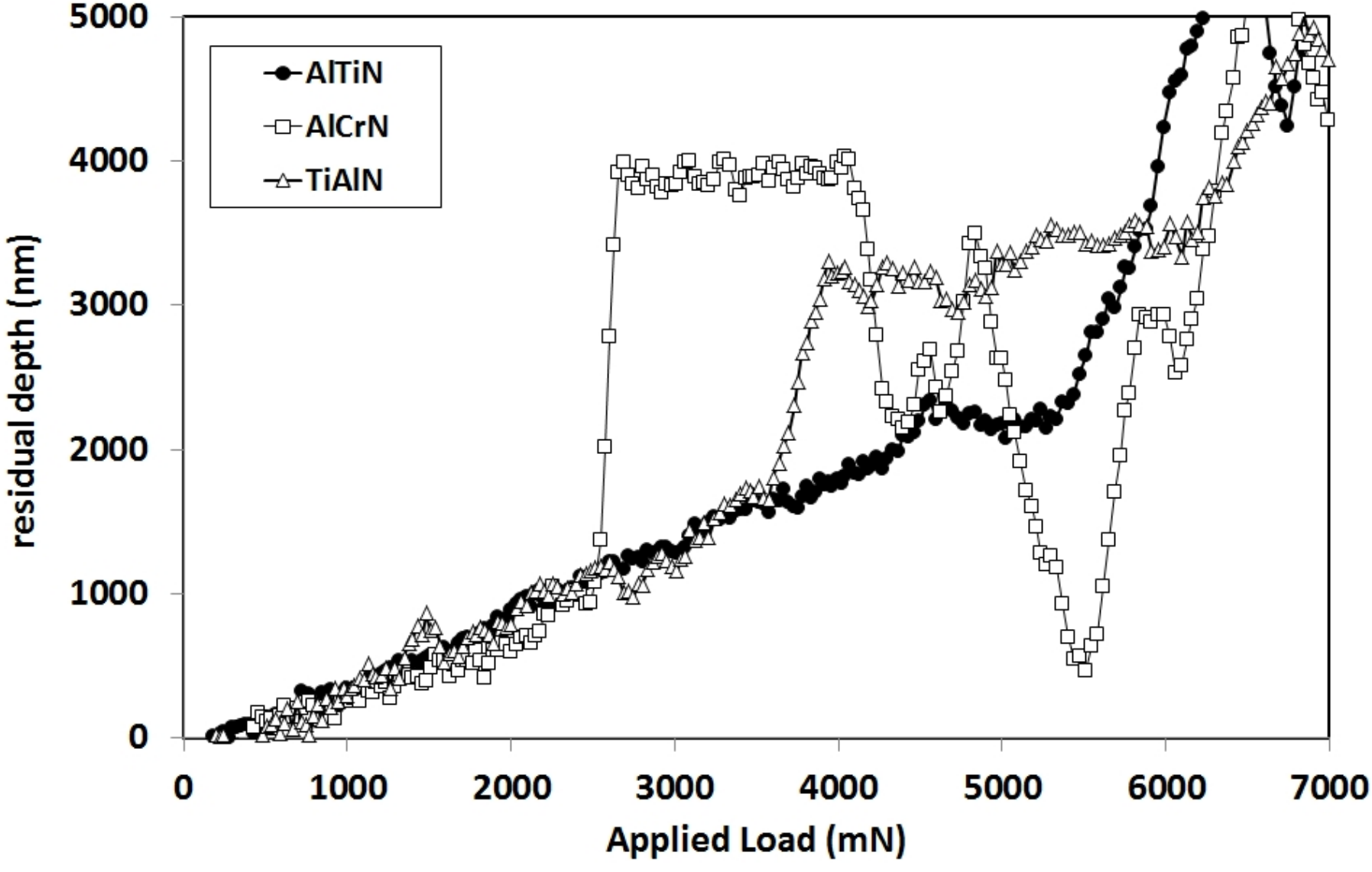
AlTiN
AlCrN
TiAlN
residual depth (nm)
0
1000
2000
3000
4000
5000
Applied Load (mN)
0
1000
2000
3000
4000
5000
6000
7000

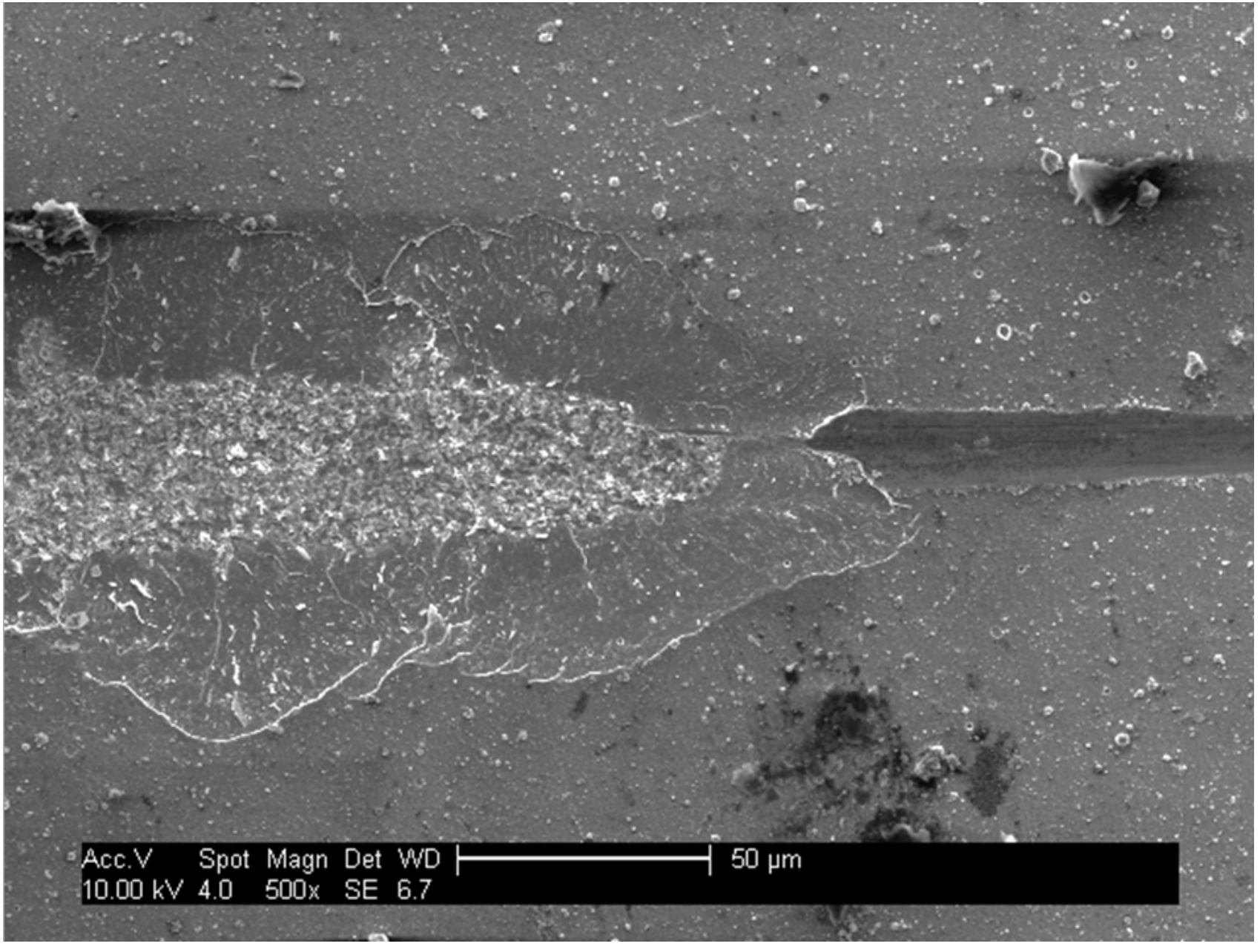
Acc.V Spot Magn Det WD
10.00 kV 4.0 500x SE 6.7
50 µm

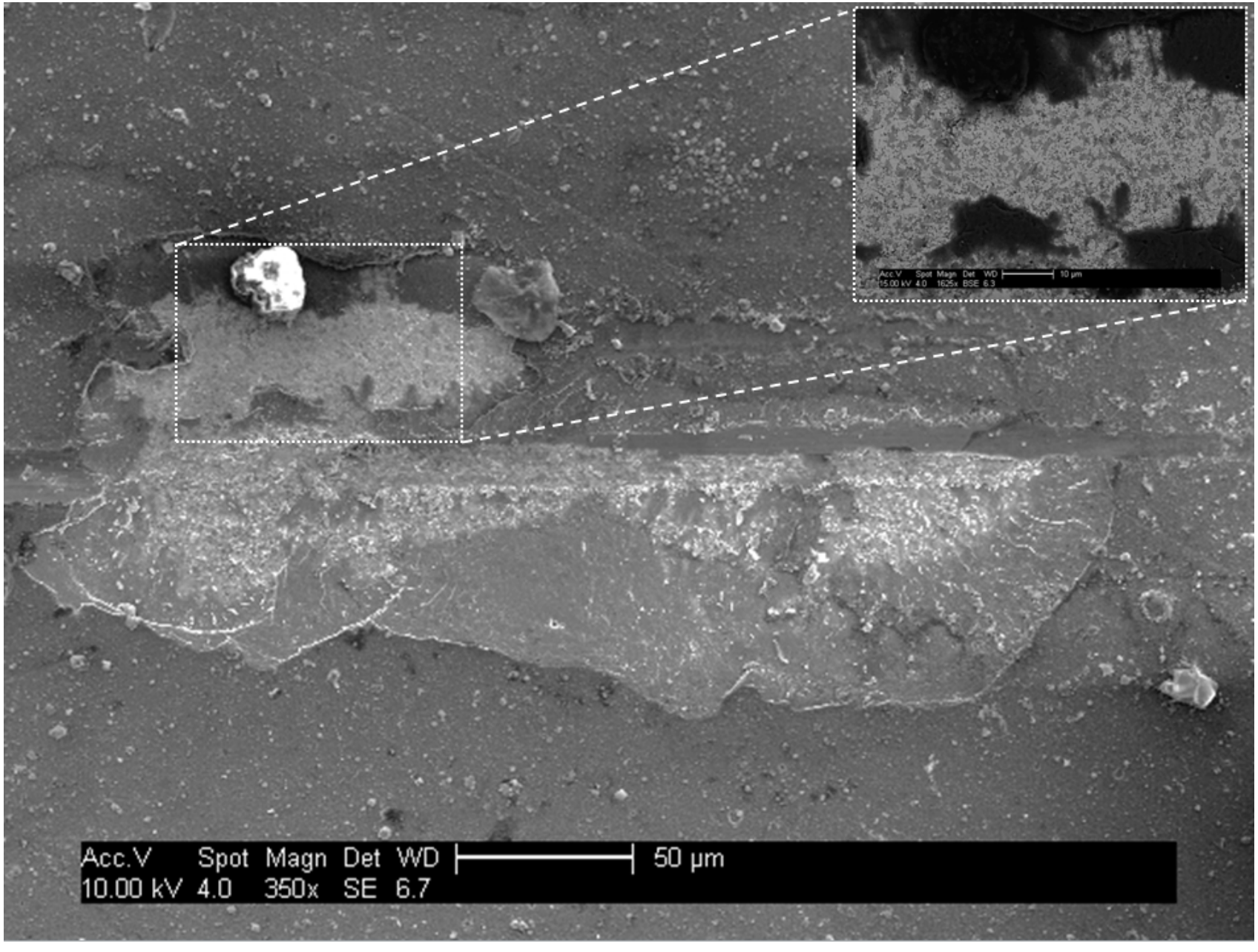
Acc.V Spot Magn Det WD
10.00 kV 4.0 350x SE 6.7
50 µm
Acc.V Spot Magn Det WD
15.00 kV 4.0 1625x BSE 8.3
10 µm

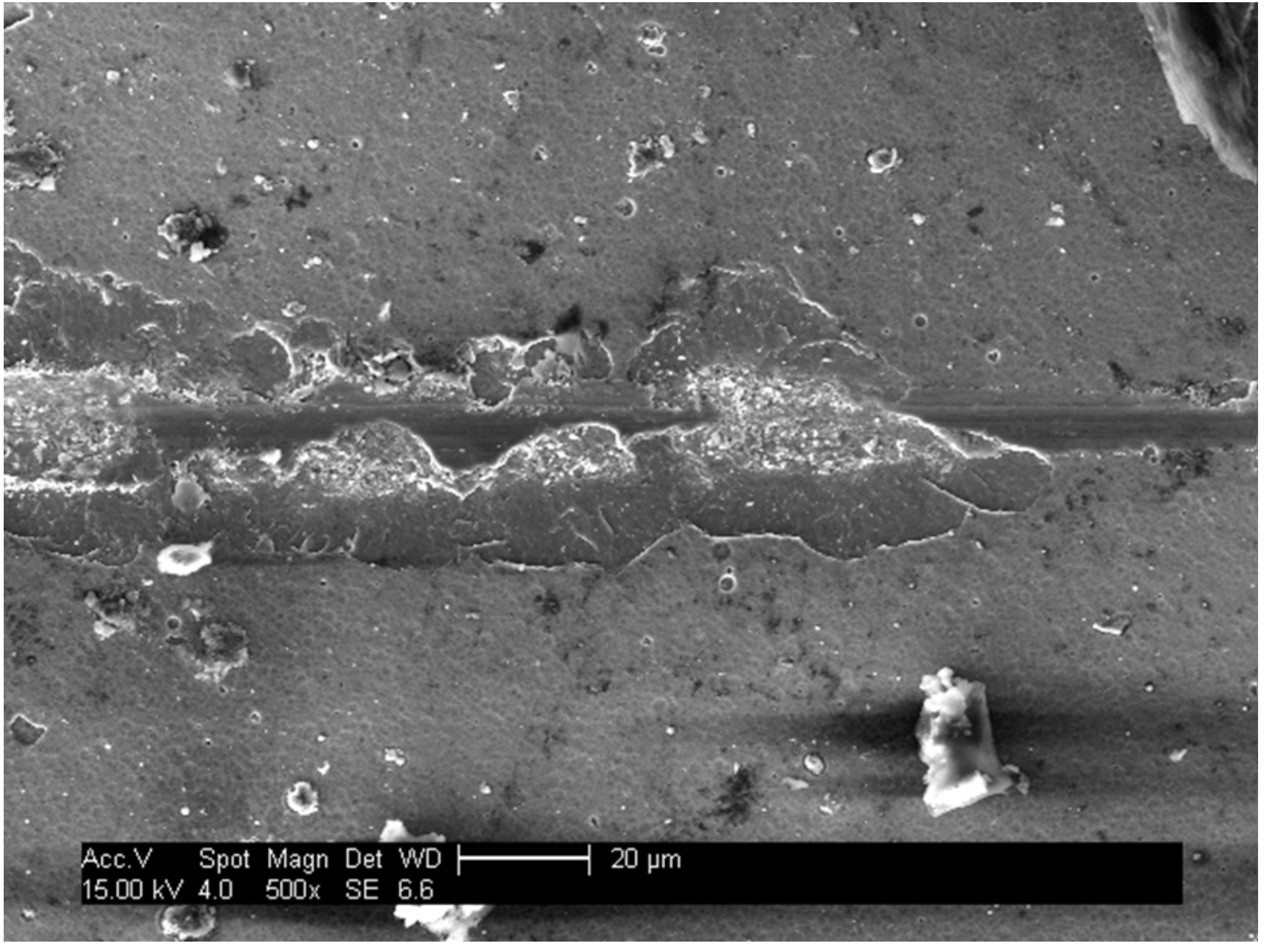
Acc.V Spot Magn Det WD 20 µm
15.00 kV 4.0 500x SE 6.6

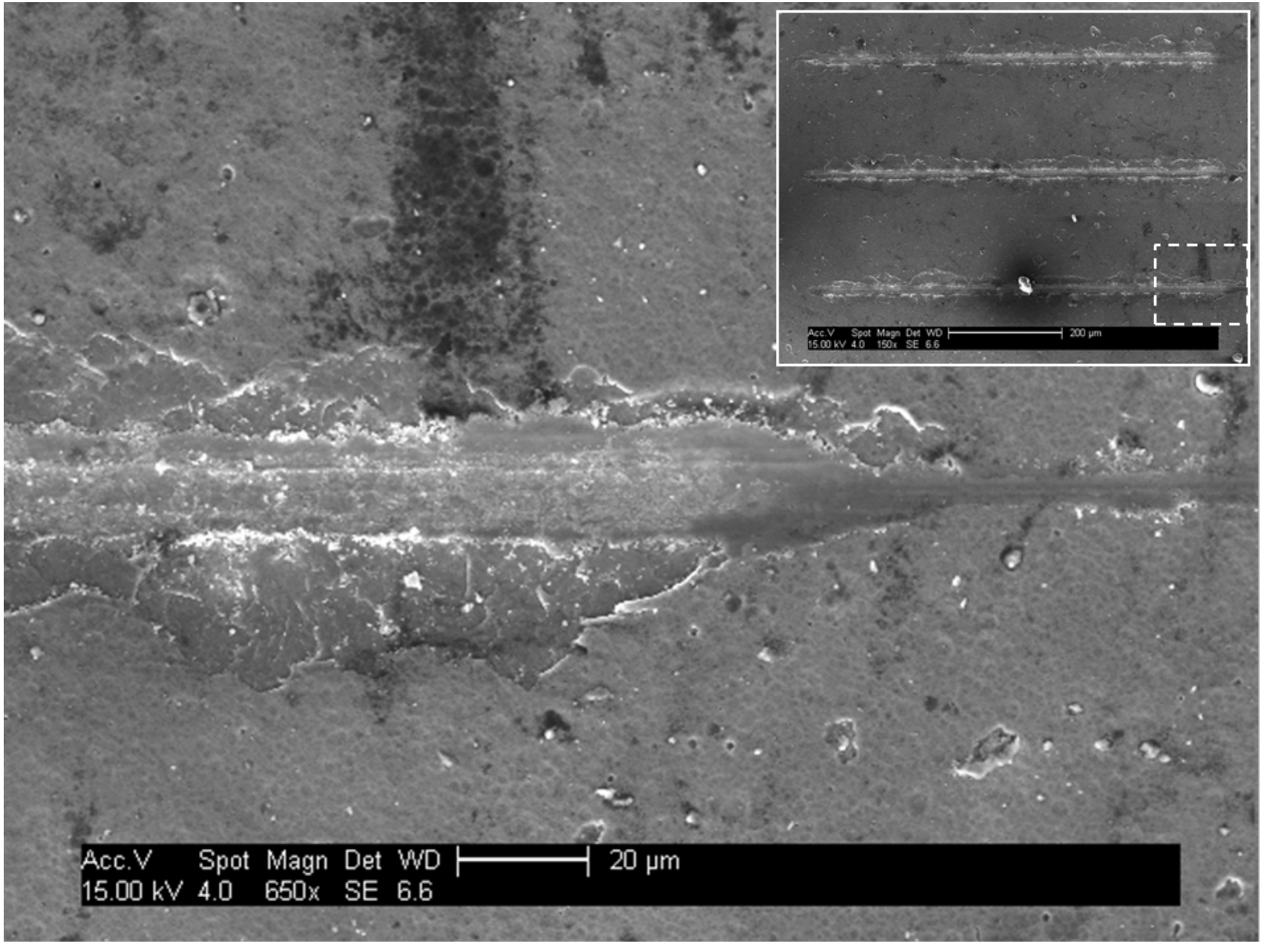
Acc.V Spot Magn Det WD 20 µm
15.00 kV 4.0 650x SE 6.6
Acc.V Spot Magn Det WD 200 µm
15.00 kV 4.0 150x SE 6.6

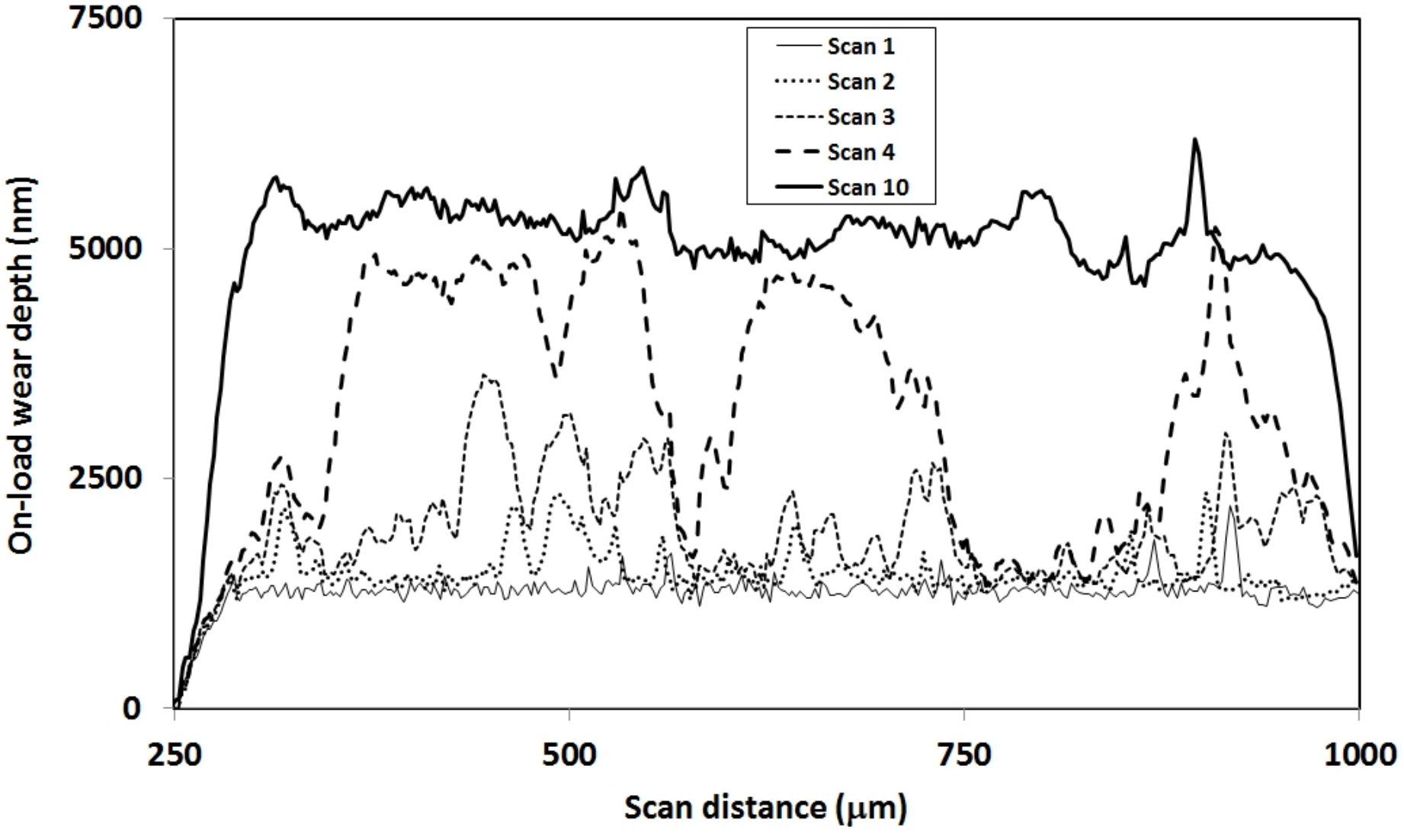
7500
5000
2500
0
On-load wear depth (nm)
250
500
750
1000
Scan distance (μm)
Scan 1
Scan 2
Scan 3
Scan 4
Scan 10

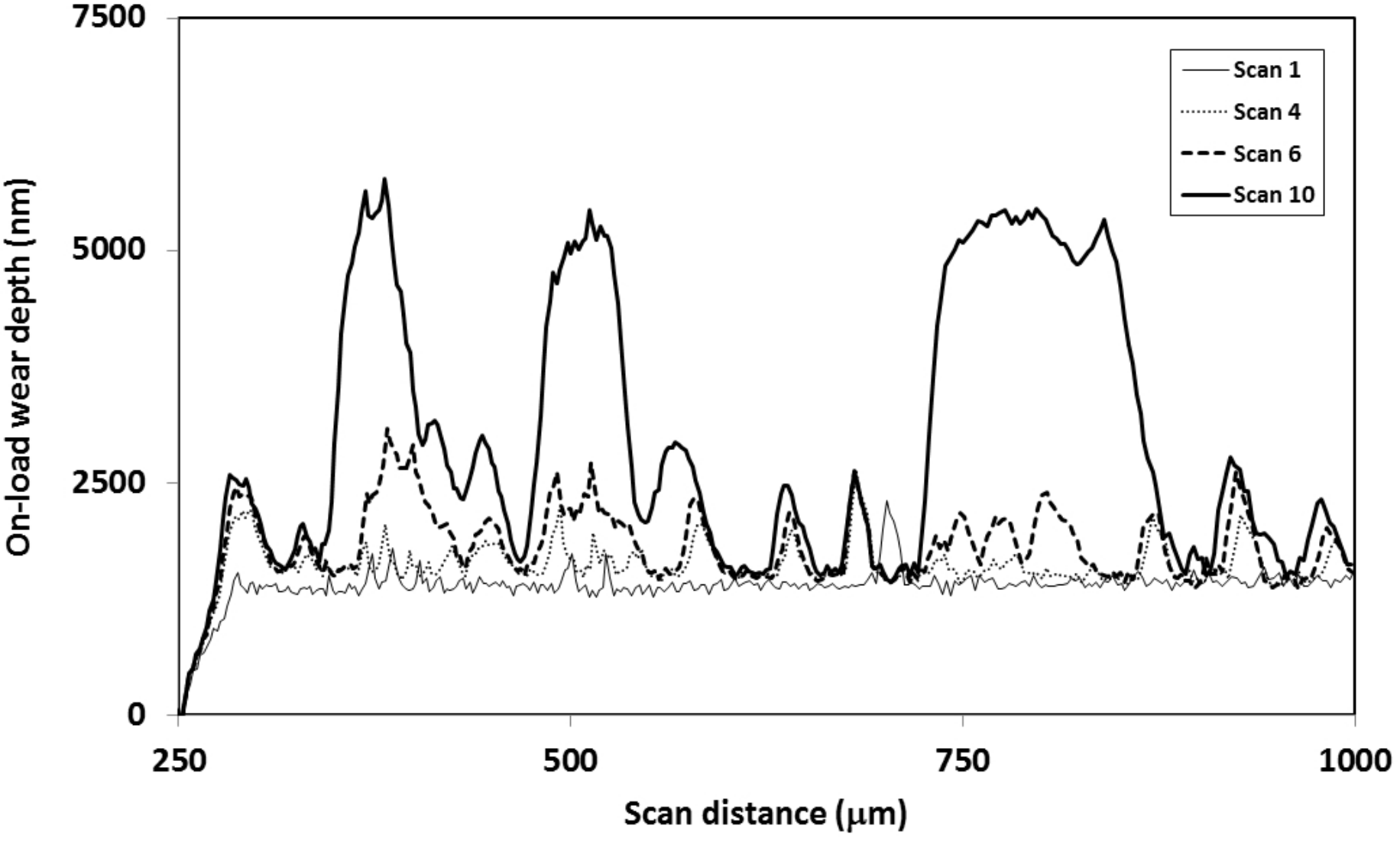
7500
5000
2500
0
On-load wear depth (nm)
250
500
750
1000
Scan distance (μm)
Scan 1
Scan 4
Scan 6
Scan 10

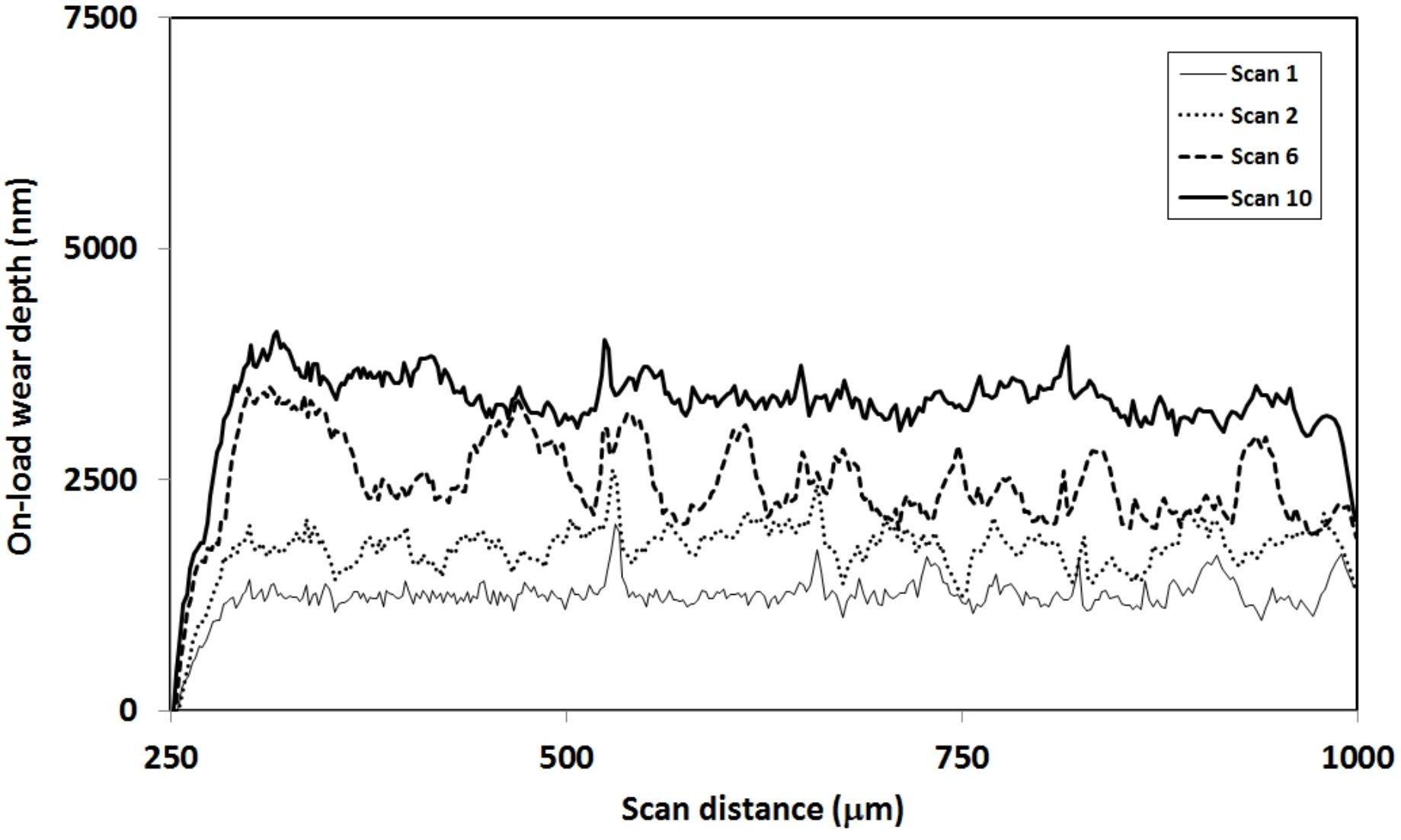
7500
5000
2500
0
On-load wear depth (nm)
250
500
750
1000
Scan distance (μm)
Scan 1
Scan 2
Scan 6
Scan 10

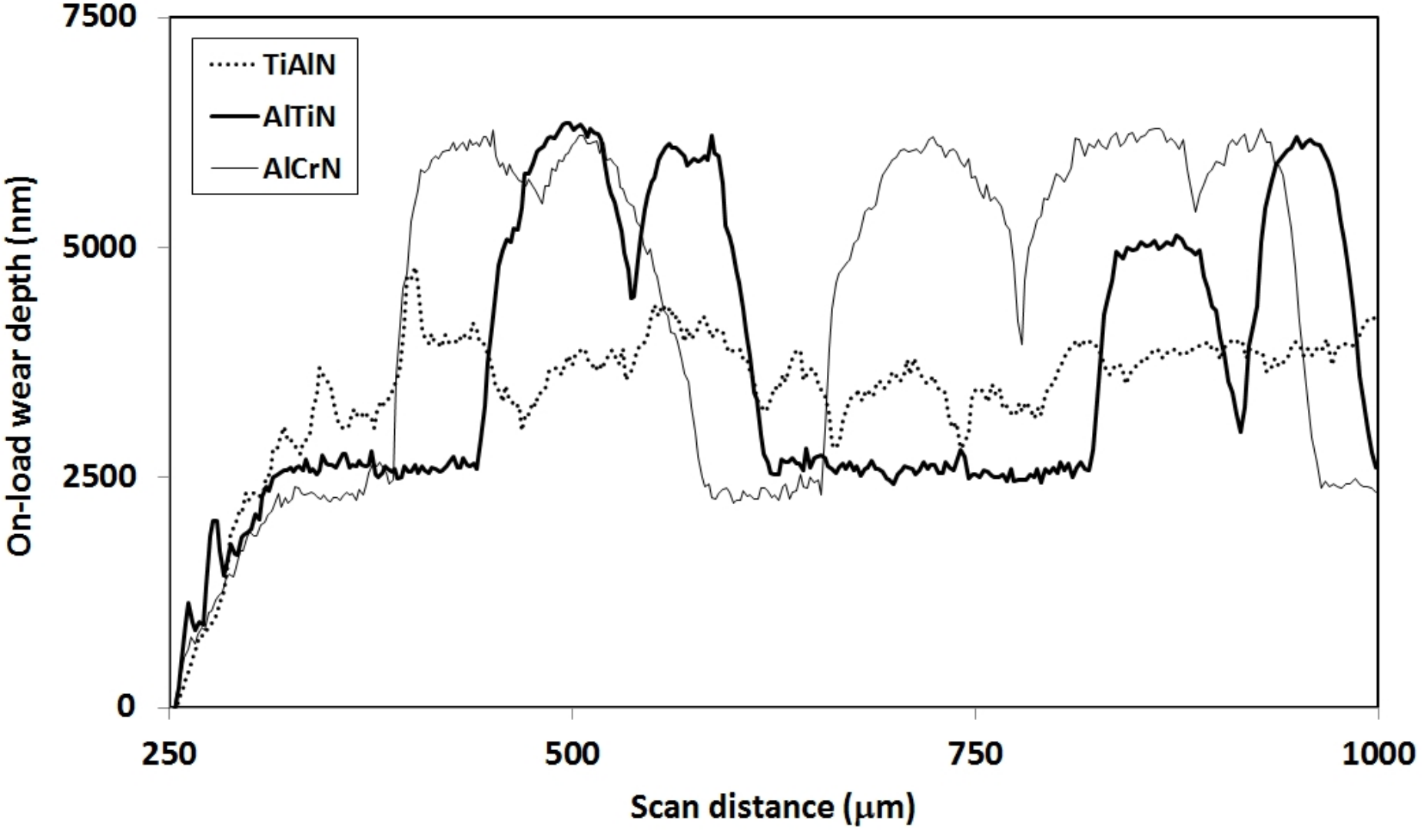
7500
5000
2500
0
On-load wear depth (nm)
TiAlN
AlTiN
AlCrN
250
500
750
1000
Scan distance (μm)

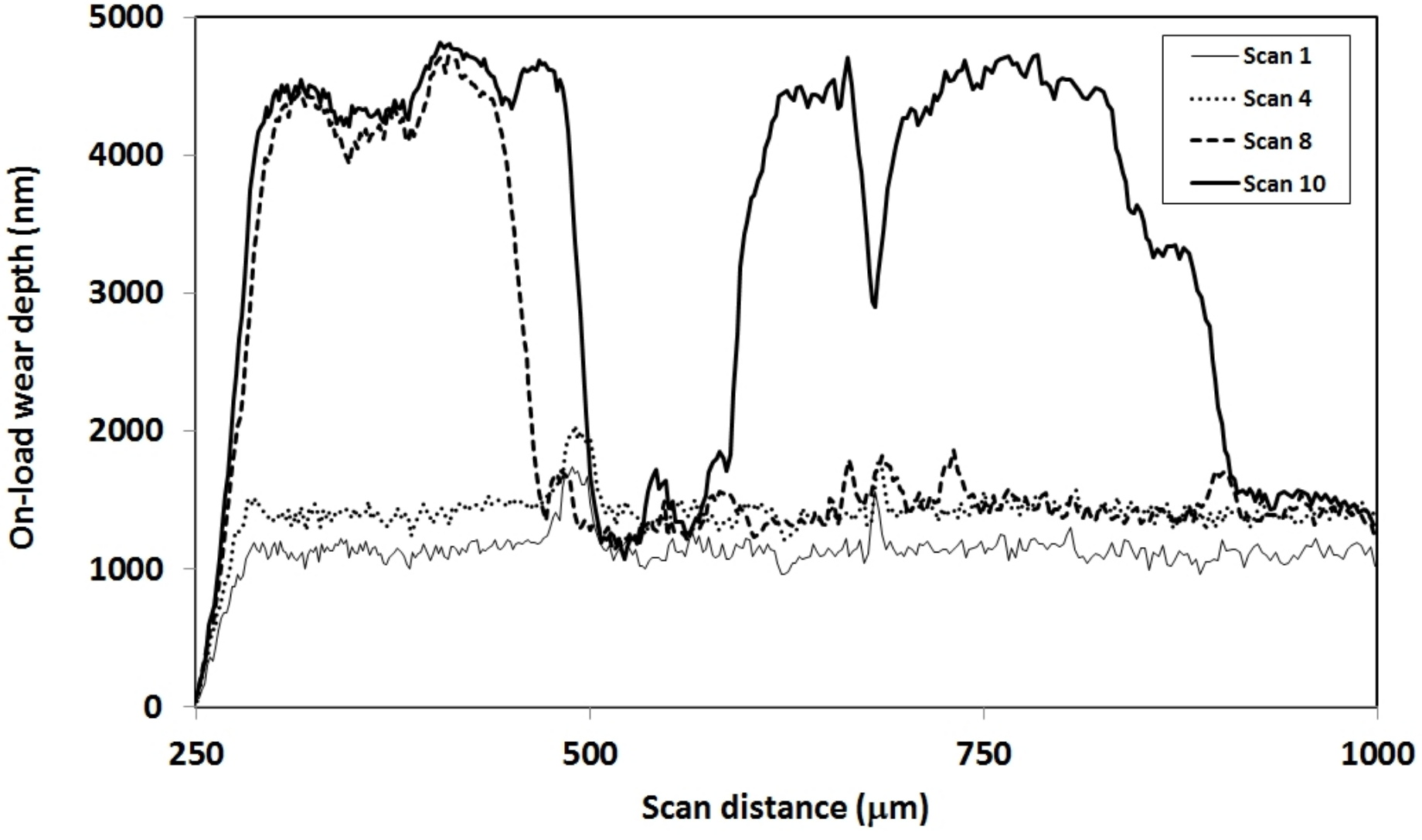
5000
4000
3000
2000
1000
0
On-load wear depth (nm)
250
500
750
1000
Scan distance (μm)
Scan 1
Scan 4
Scan 8
Scan 10

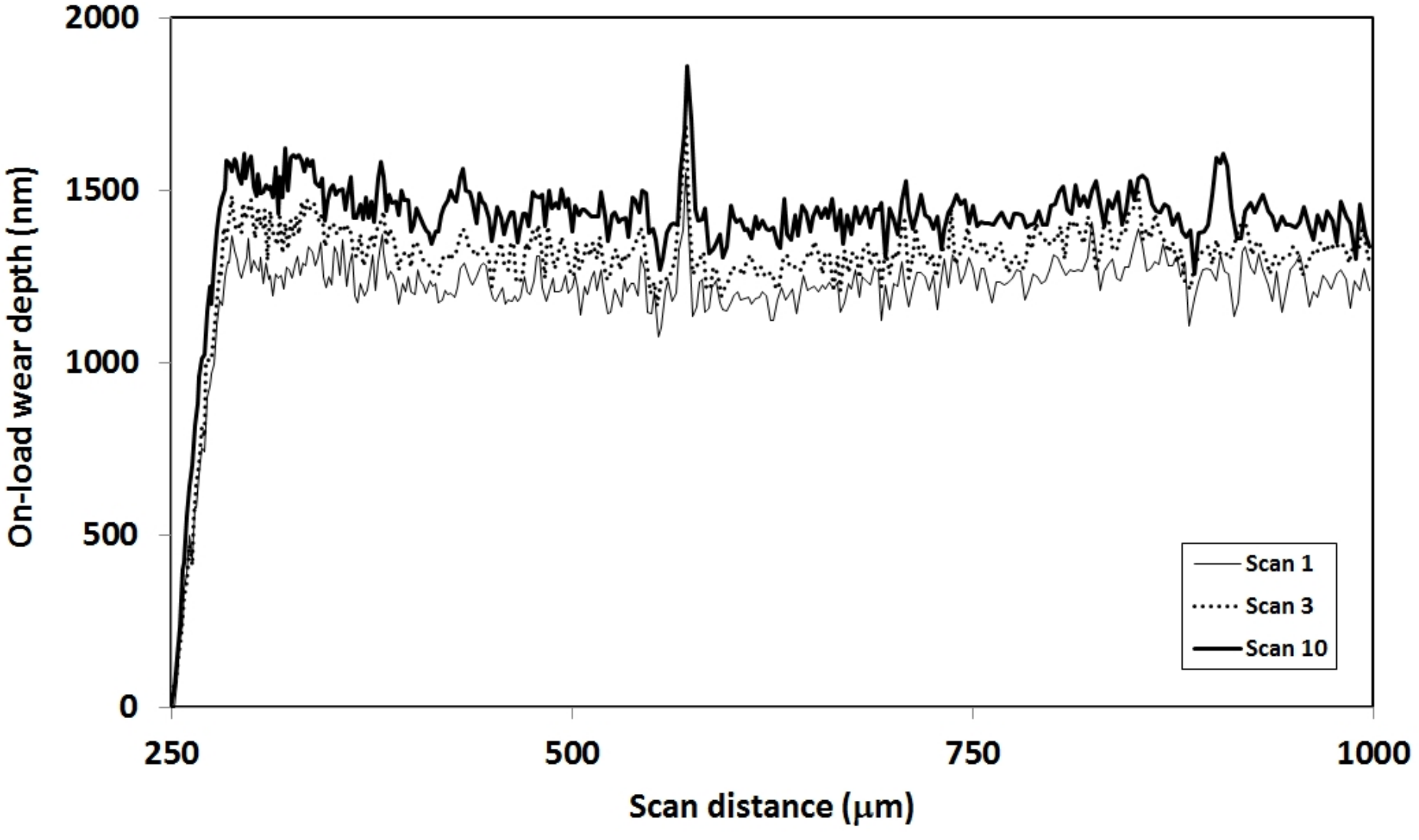
2000
1500
1000
500
0
On-load wear depth (nm)
250
500
750
1000
Scan distance (μm)
Scan 1
Scan 3
Scan 10

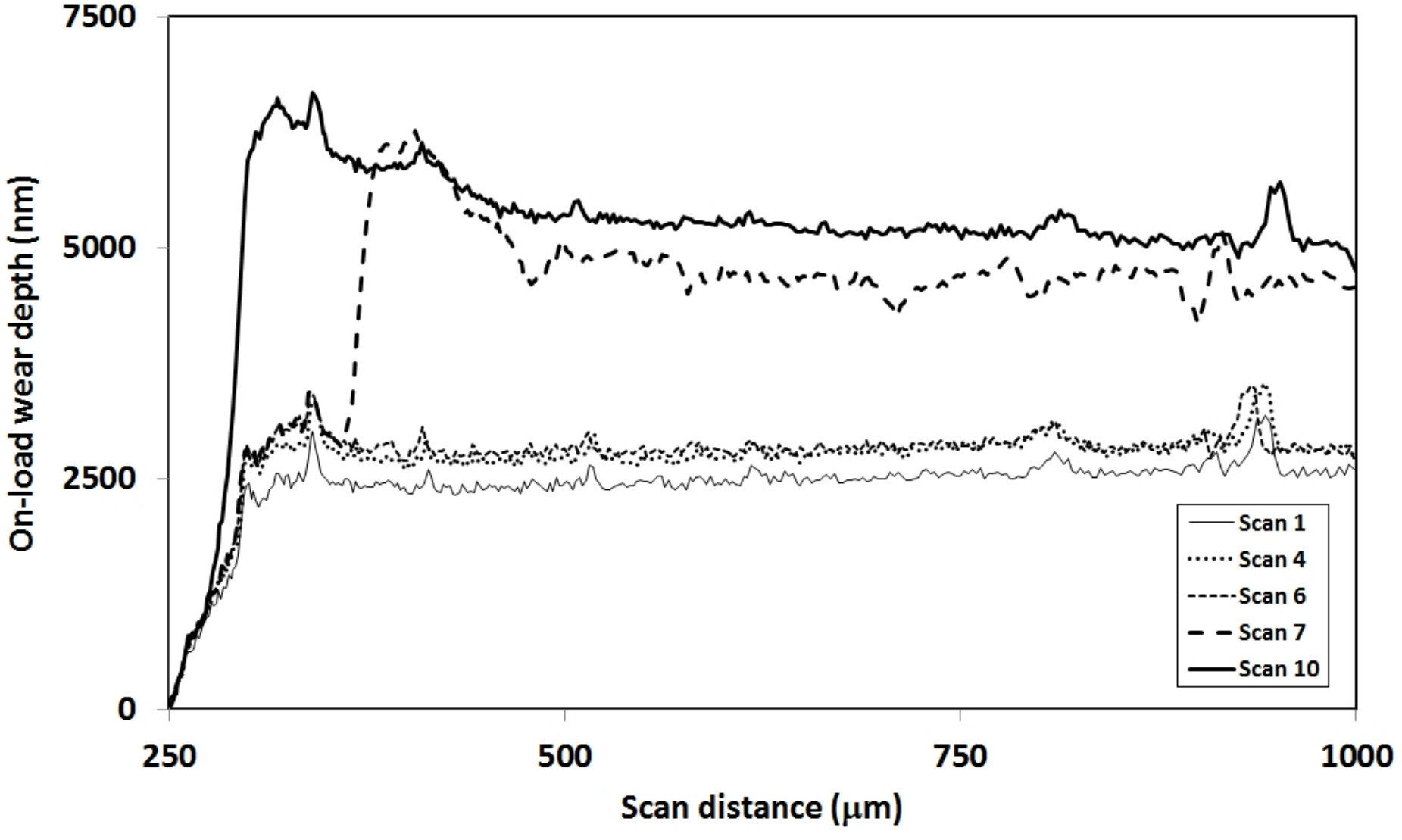
7500
5000
2500
0
On-load wear depth (nm)
250
500
750
1000
Scan distance (μm)
Scan 1
Scan 4
Scan 6
Scan 7
Scan 10

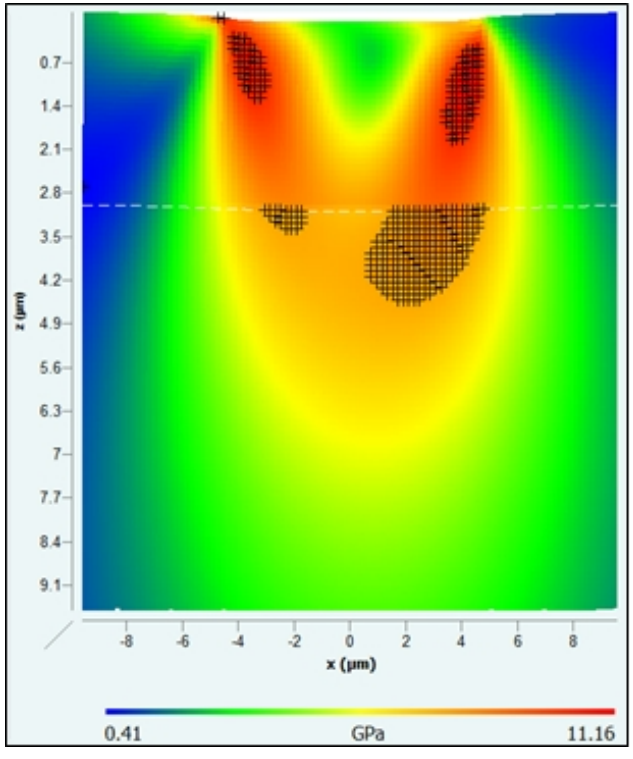
z (µm)
0.7
1.4
2.1
2.8
3.5
4.2
4.9
5.6
6.3
7
7.7
8.4
9.1
-8 -6 -4 -2 0 2 4 6 8
x (µm)
0.41 GPa 11.16

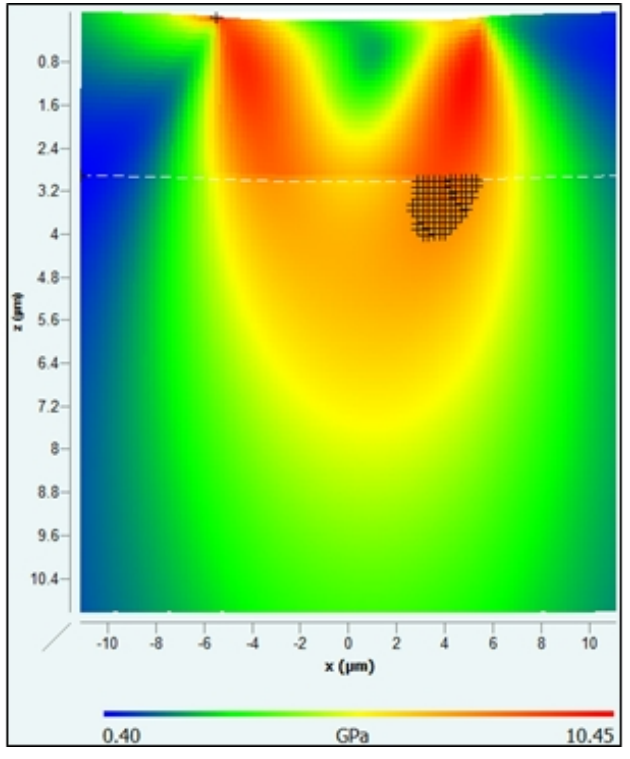
z (µm)
0.8
1.6
2.4
3.2
4
4.8
5.6
6.4
7.2
8
8.8
9.6
10.4
-10 -8 -6 -4 -2 0 2 4 6 8 10
x (µm)
0.40 GPa 10.45

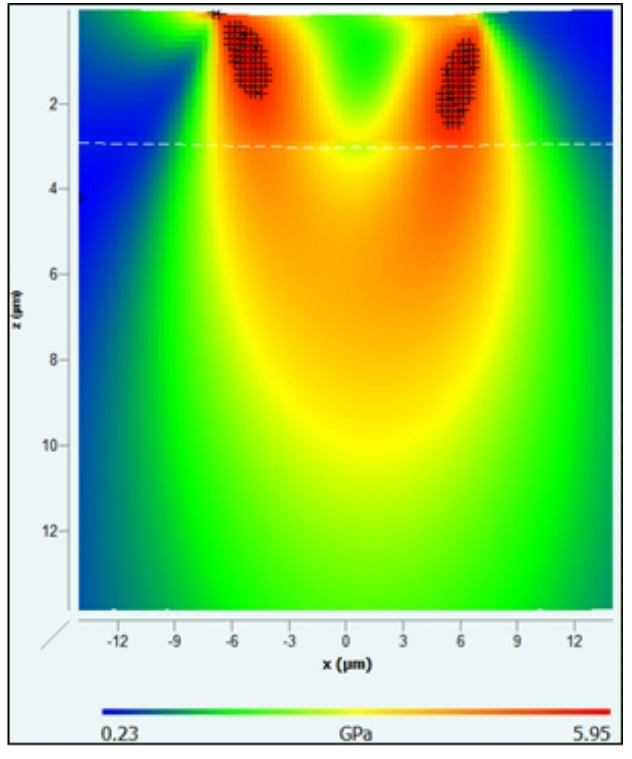
z (µm)
2
4
6
8
10
12
-12 -9 -6 -3 0 3 6 9 12
x (µm)
0.23 GPa 5.95

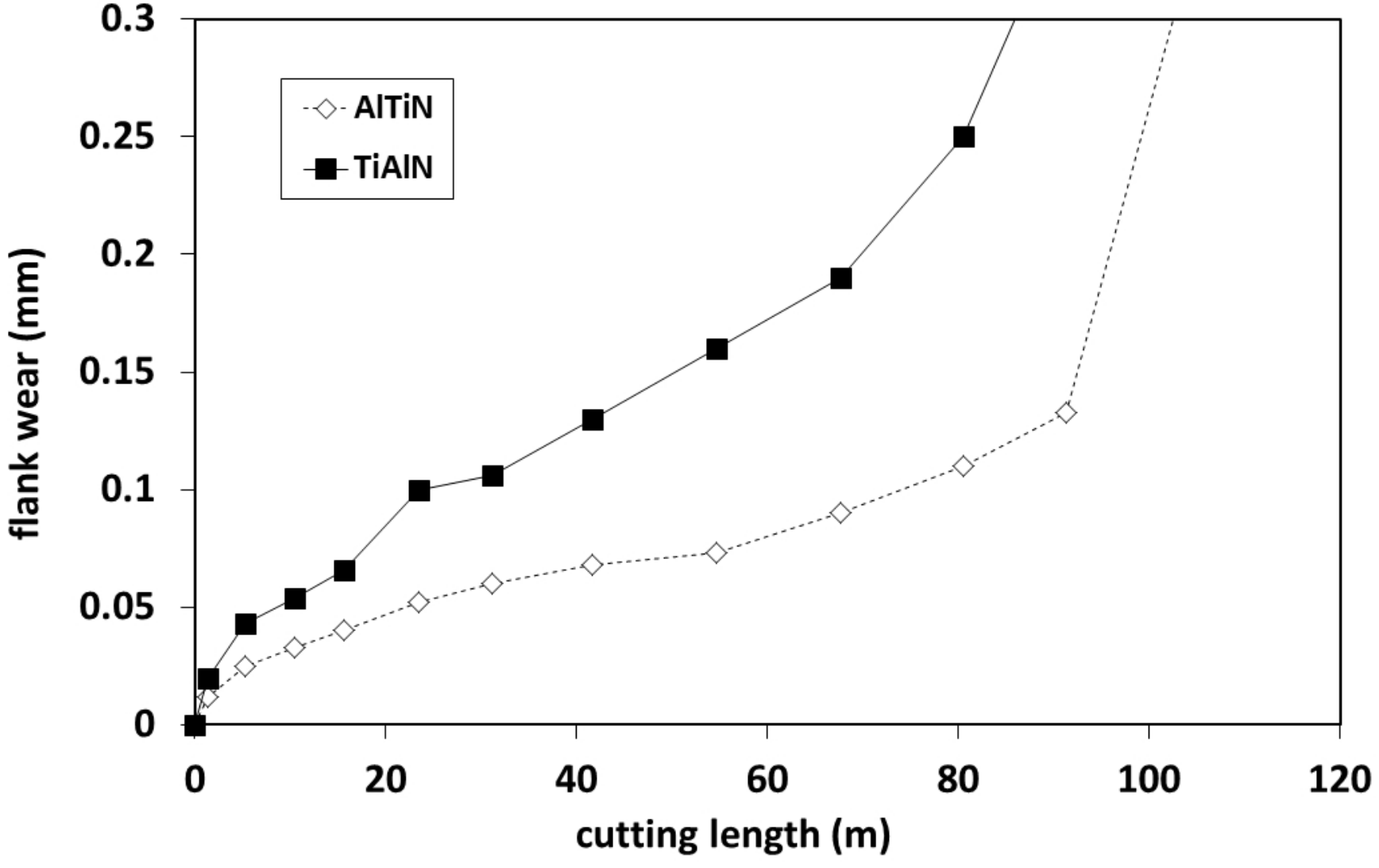
AlTiN
TiAlN
flank wear (mm)
0.3
0.25
0.2
0.15
0.1
0.05
0
0
20
40
60
80
100
120
cutting length (m)

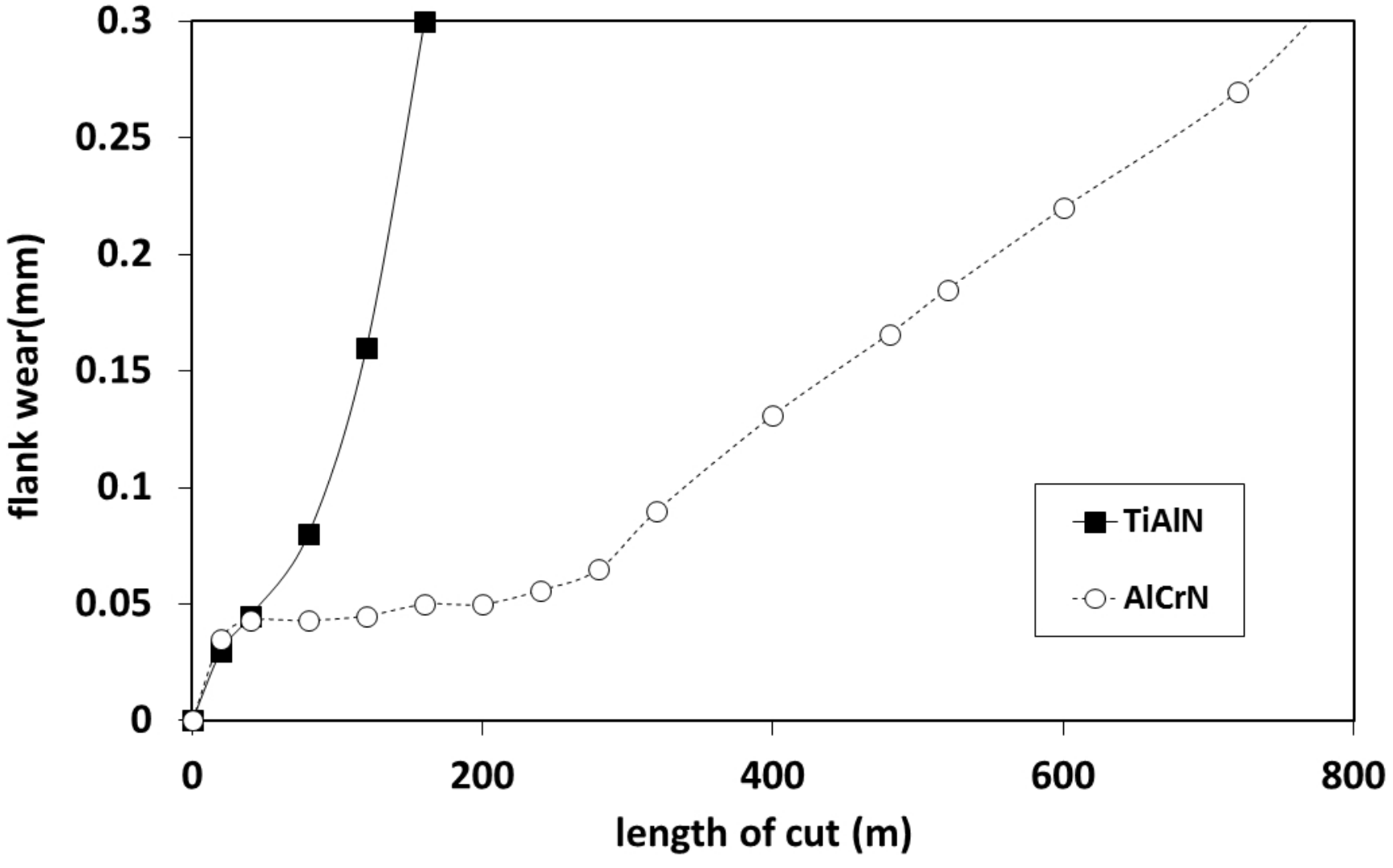
0.3
0.25
0.2
0.15
0.1
0.05
0
flank wear(mm)
0
200
400
600
800
length of cut (m)
TiAlN
AlCrN

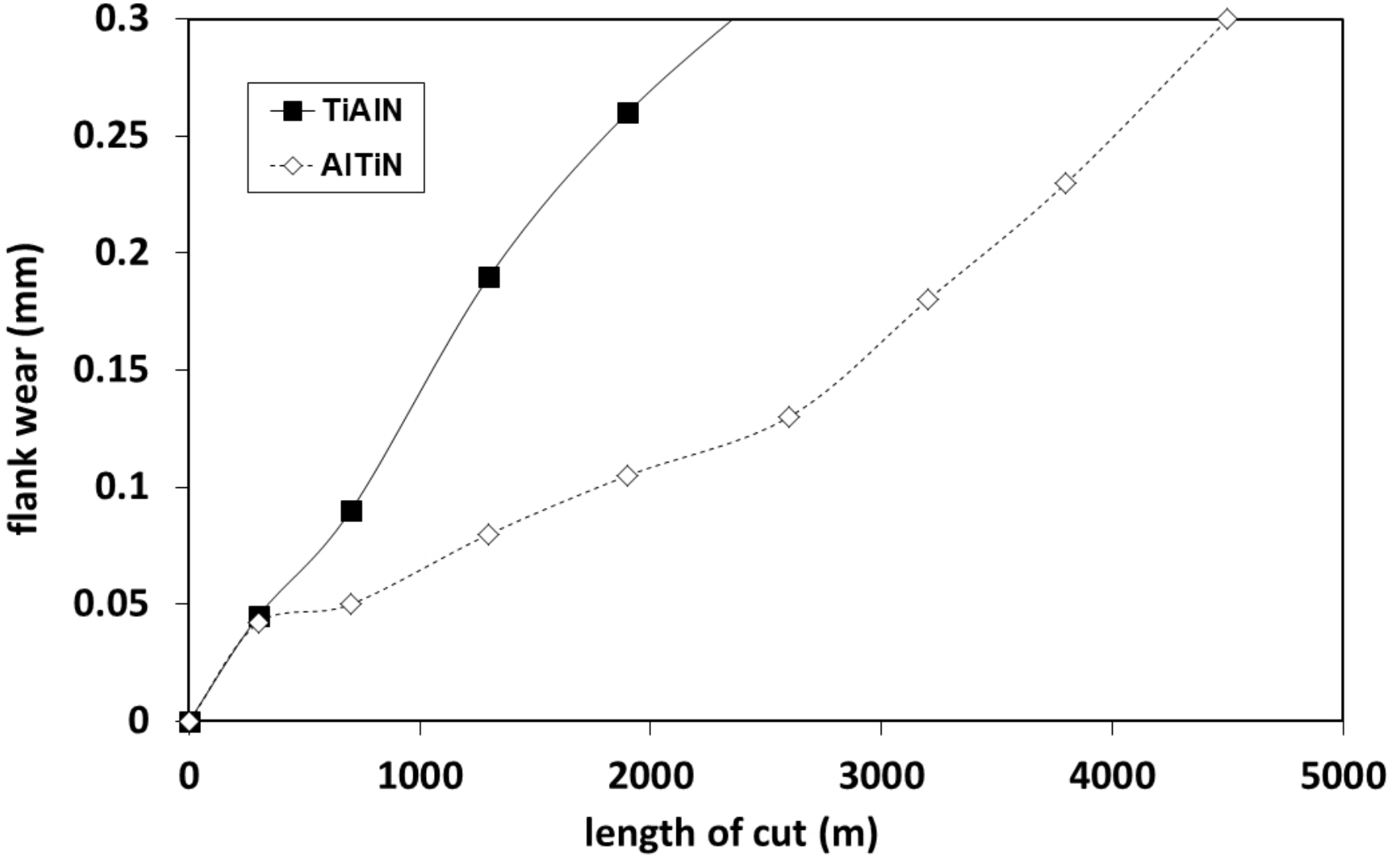
0.3
0.25
0.2
0.15
0.1
0.05
0
flank wear (mm)
TiAlN
AlTiN
0
1000
2000
3000
4000
5000
length of cut (m)

Elevated temperature repetitive micro-scratch testing of AlCrN, TiAlN and AlTiN PVD coatings

Beake, Ben D.

2017-08-24

B.D. Beake, J.L. Endrino, C. Kimpton, G.S. Fox-Rabinovich, S.C. Veldhuis, (2017) Elevated temperature repetitive micro-scratch testing of AlCrN, TiAlN and AlTiN PVD coatings, International Journal of Refractory Metals and Hard Materials, Volume 69, December 2017, pp. 215-226
https://doi.org/10.1016/j.ijrmhm.2017.08.017